CARBON MONOXIDE CHEMICAL LASER RESEARCH

William Q. Jeffers

McDonnell Douglas Research Laboratories

Prepared for:

Advanced Research Projects Agency

1 September 1972

(1)

MCDONNELL DOUGLAS RESEARCH LABORATORIES

MCDONNELL DOUGLAS CORPORATION

Carbon Monoxide Chemical Laser Research

Second Quarterly Technical Report

Contract No. DAAH01-72-C-0578

1 June 1972 - 1 September 1972

Sponsored by:
Advanced Research Projects Agency
ARPA Order No. 1256
Project No. PAN RX 12

Monitored by:
U. S. Army Missile Command
Redstone Arsenal, Alabama 35809

Project Scientist:
William Q. Jeffers
Radiation Sciences Department
(314) 232-4687

MCDONNELL DOUGLAS RESEARCH LABORATORIES

Box 516, Saint Louis, Missouri 63166 (314) 232-0232

MCDONNELL DOUGLAS
CORPORATION

(56)

CONTENTS

ABSTRACT

This report describes the research accomplished in the second quarter of the program entitled "CO Chemical Laser Research". Briefly, the objectives of this research are to experimentally study single line operation of a CO chemical laser, and to develop a theory of cw CO chemical lasers.

The first task of the program, a demonstration of single line operation of a cw CO chemical laser, was completed in the first quarter and reported in the First Quarterly Progress Report (23 February 1972 - 1 June 1972).

The theoretical treatment of the cw CO chemical laser (Task 3) is the main subject of this report. In order to investigate the collisional relaxation effects occurring in CO chemical laser media, the master relaxation equations for CO-M systems were solved by computer calculations. The relaxation of CO* from the O + CS chemical reaction distribution, was studied for the cases of CO*, CO*-He, CO*-O_2, CO*-CO(300 K), and CO*-O_2 + CO(300 K). Unless a large excess of some collision partner is present (CO*:M of 1:100 or more), the dominant collisional relaxation phenomena will be CO*-CO* or CO*-CO(300 K) processes.

The complete theory, including fluid flow, chemical kinetics, relaxation, and optical properties, is described in detail. The zero optical intensity theory is used to model the MDRL CO chemical laser for two cases of interest: with and without CO(300 K) injection into the reacting stream. The results agree in general with

experiment, but predictions of R-branch gains from the theory suggest that the published CO* distribution formed by the O + CS pumping reaction has a limited range of validity.

I. INTRODUCTION

This report describes progress made in the second quarter (1 June 1972 - 1 September 1972) on the program "CO Chemical Laser Research" at the McDonnell Douglas Research Laboratories (MDRL).

The technical objectives of this contract are as follows:

Task 1. Experimental demonstration of single line operation with a cw CO chemical laser based on the $O + CS_2$ reaction.

This task was completed in the first quarter and the results reported in the First Quarterly Contract Report (23 February 1972 - 1 June 1972).[1]

Task 2. Experimental study of the effects of various parameters on single line output power for the chemical laser of Task 1.

This task is in progress and results will be reviewed in subsequent reports.

Task 3. Formulation of a theory of the cw CO chemical laser to calculate both zero intensity parameters and the interaction of the stimulated optical fields with the active medium.

The theory of cw CO chemical lasers has been completed for the zero intensity case. This theory and results obtained from computer calculations with it will be the main subject of the present report.

The principal investigator is W. Q. Jeffers. R. F. Webbink and F. S. Skinner also participated in this effort in the second quarter.

II. PROGRESS AND RESULTS

Task 3

2.1 Collisional Relaxation of CO*

Our effort on the theoretical description of cw CO chemical lasers was directed to two major problems in the second quarter. In the first problem, we have programmed the master relaxation equations for CO-M mixtures. The program, called RELAX 1, takes an arbitrary initial distribution of CO in excited states up to v = 50 and calculates the subsequent distributions which evolve by single quantum V-V, V-T, and spontaneous emission processes. The V-V and V-T processes are included for CO-CO and CO-M collisions where M is either a monatomic or diatomic species. In the case where M is diatomic, the M distribution is assumed to be in thermal equilibrium at the gas kinetic temperature which is constant at 300 K.

Transition probabilities for CO-M collisions (M = CO, He, O_2) for both V-V and V-T energy transfers have been calculated by our previously-developed techniques.[2,3] The V-V calculations for CO-CO exchanges,

$$CO(v) + CO(v') \rightarrow CO(v \pm 1) + CO(v' \mp 1) \qquad (1)$$

have been done for both long-range and short-range interactions, and for $(v,v') \leq 50$. The transition probabilities from the short-range interactions are limited to values of 0.125 by the theory.[3] The long-rang interactions are treated by a perturbation theory result, and we have set an upper limit on the calculated probabilities, P, by using a pseudo-probability P' defined by

$$P' = \frac{P}{1 + eP} \qquad (e = 2.71828 \ldots) \tag{2}$$

The V-T exchange with He was treated using the standard SSH theory[4] of V-T transfer. The calculated results for

$$CO(v) + He \rightarrow CO(v - 1) + He \tag{3}$$

were adjusted to experimental data[5] by a scale factor. The exchange with O_2 was also treated in the relaxation equations as a V-T collision, but the probability for this event,

$$CO(v) + O_2(0) \rightarrow CO(v - 1) + O_2(1) \tag{4}$$

was calculated from the V-V theory for short-range interactions.[3] Again, the computed results were adjusted to experimental data[5] by a scale factor.

The first calculation done was the case for chemically-formed CO relaxing from the initial distribution of the O + CS reaction.[6] This reaction is well established as the pumping step in CO chemical lasers,[7] and its distribution has been deduced from at least two different experiments.[5,6] The relaxation calculation includes CO-CO V-V and V-T processes as well as spontaneous emission.[8] This calculation assumes that n, the total density of CO, is 3.215×10^{15} cm^{-3} and is distributed in the excited states as shown in the t = 0 curve of Fig. 1. This distribution represents a slight smoothing of the distribution obtained experimentally by Hancock and Smith.[6] Figures 1-5 display the results as functions of both vibrational quantum number v and time t.

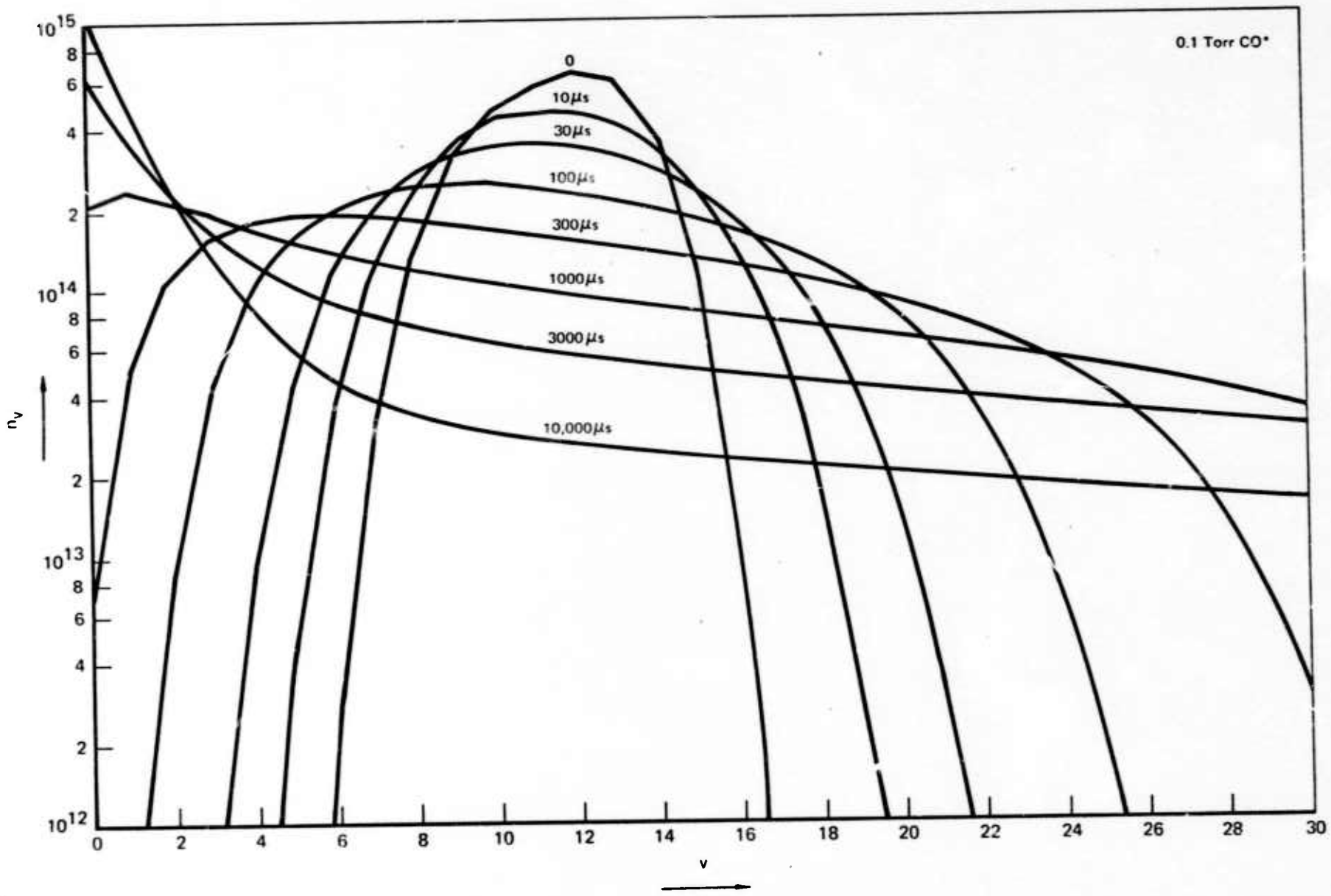

Fig. 1 Relaxation of chemically-formed CO* at P = 0.1 Torr, T = 300 K.

In general, relaxation from the peaked chemical distribution is rapid. Population spreads to both higher and lower levels and tends to form a flat distribution at intermediate times ($t \leq 1000$ μsec). At longer times the distribution could be described by a low vibrational temperature at low v ($v \leq 6$) and a high vibrational temperature at high v ($v \geq 7$). Figure 2 is a plot of maximum (with respect to J) P-branch gains α_P which exist on each vibrational transition. There is a rapid decrease in the gains on the bands directly excited by the chemical reaction. Bands at low and high vibrational levels build up gain as the population distribution spreads, and subsequently relax back toward smaller gains. R-branch gains α_R exist only on the positive slope side of the chemical distribution (Fig. 3), spread toward low v, and decrease rapidly. Even though V-V transfer removes no quanta from the system, the redistribution decreases the optical gain coefficients. All of these effects can be seen again in Figs. 4 and 5 in the time-dependence of the maximum P- and R-branch gains. It is clear that CO-CO V-V transfer is a rapid mode of redistribution of population from the chemically-formed distribution.

In order to evaluate the effects of various collision partners which would be present in a real CO chemical laser, calculations were run for the chemical distribution again with $n_{total} = 3.215 \times 10^{15}$ cm^{-3} (corresponding to P = 0.1 Torr) and with 1.0 Torr of He, O_2, and "cold" CO. The calculations were run independently to separate the effects of the various collision partners. Figures 6 and 7 show the results of the CO*:He (1:10) calculation. Both the distributions and gain coefficients are negligibly different from the case with

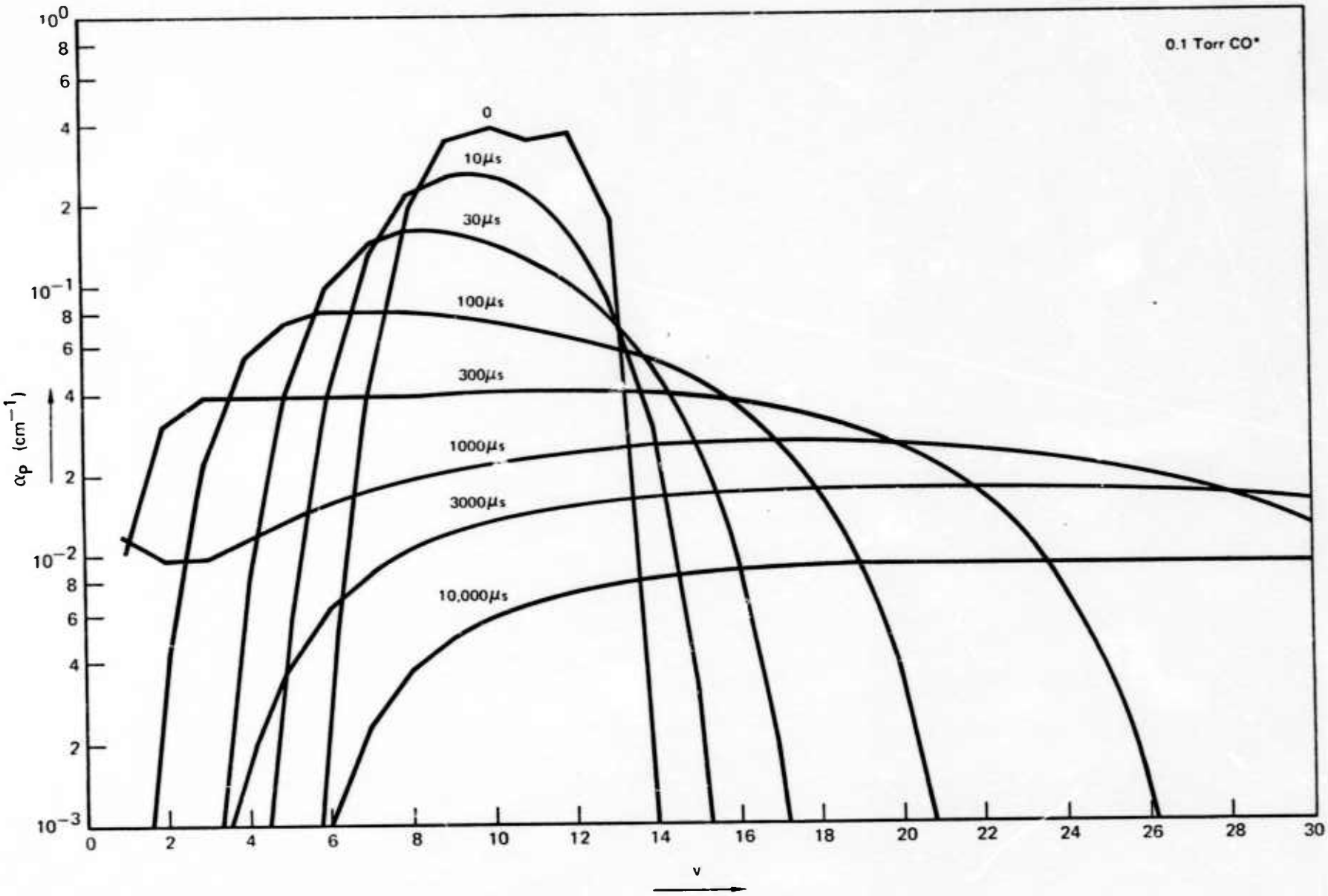

Fig. 2 Maximum P-branch gain coefficients α_p resulting from the time-dependent distributions of Fig. 1.

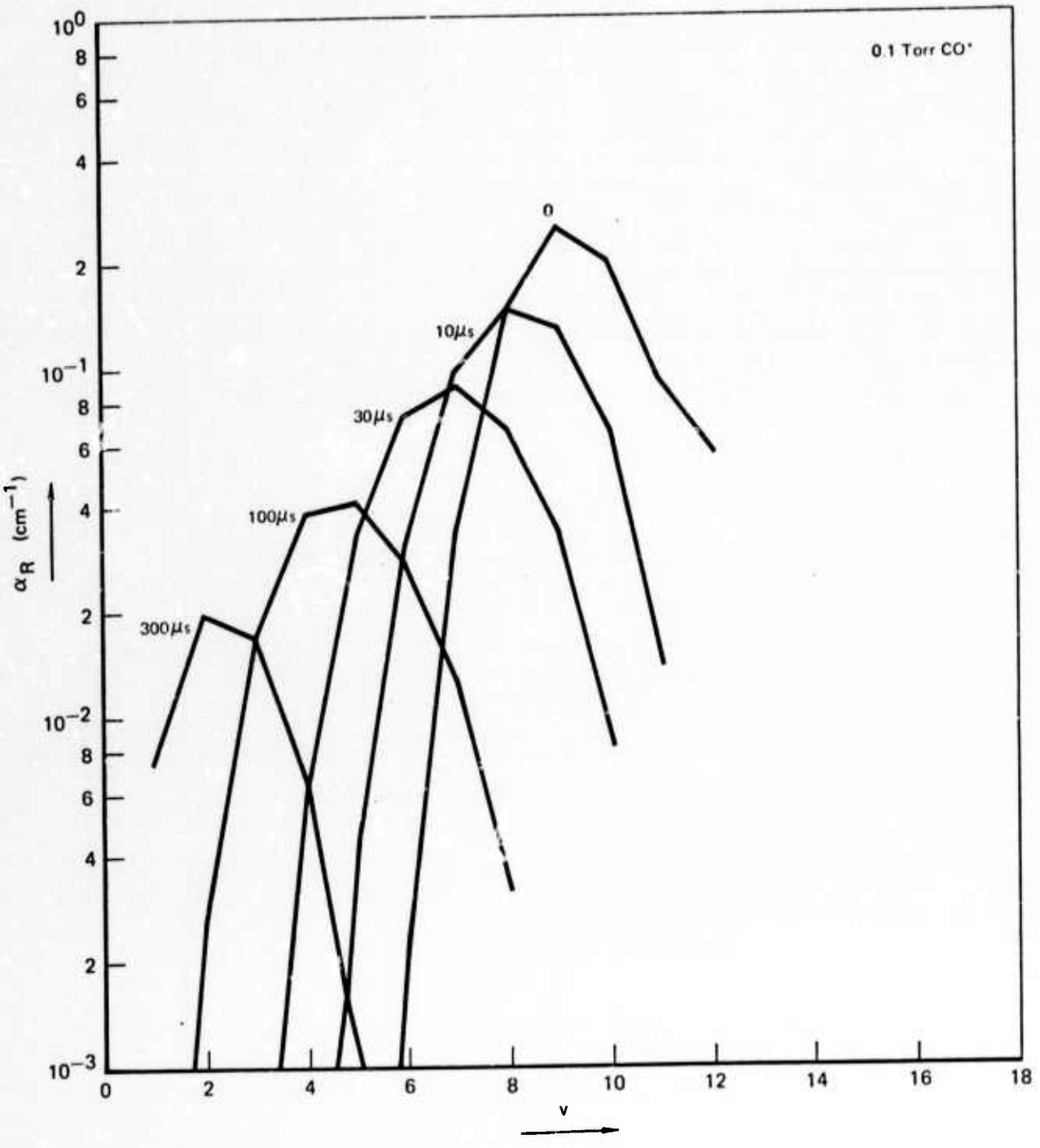

Fig. 3 Maximum R-branch gain coefficients α_R resulting from the time-dependent distributions of Fig. 1.

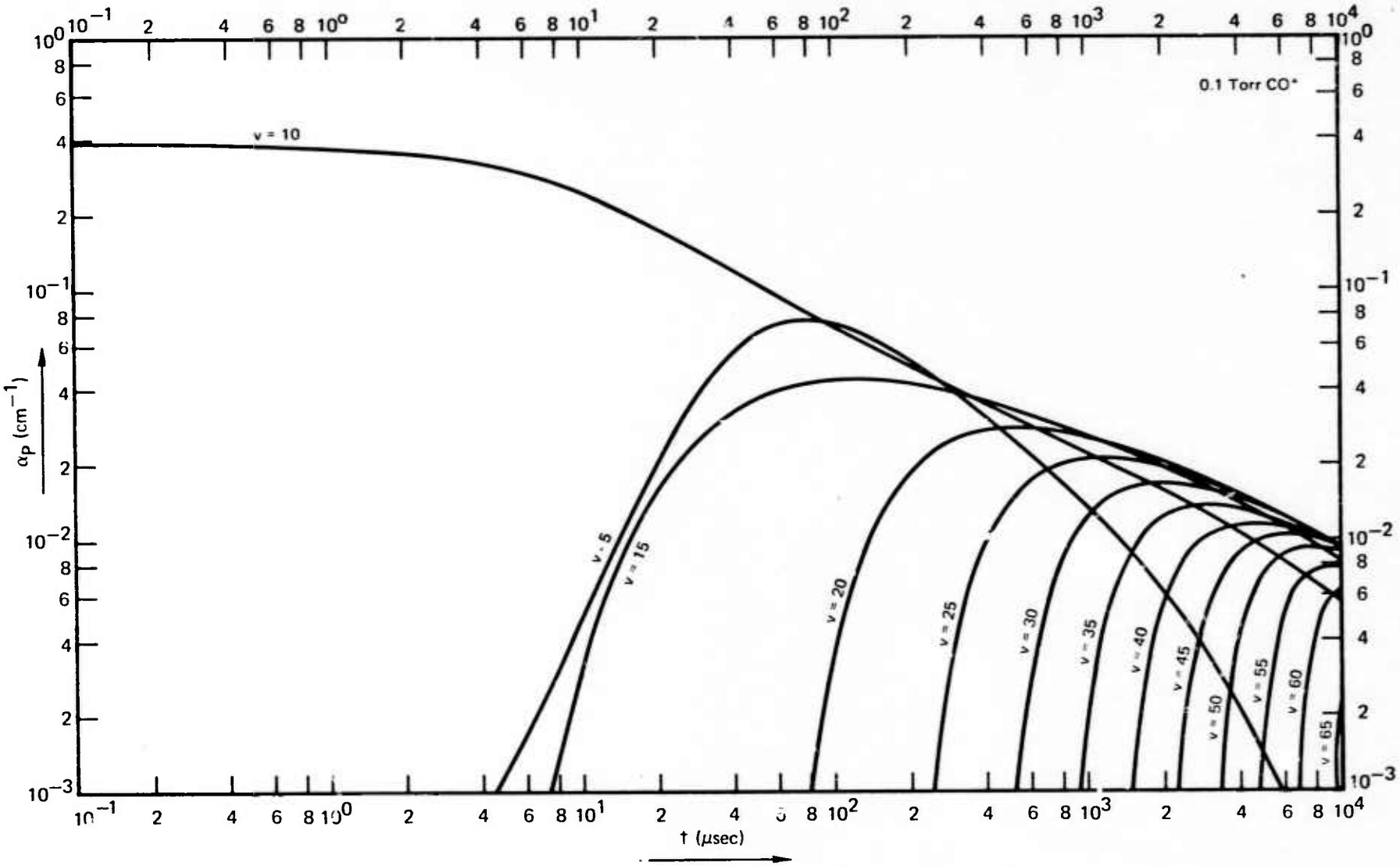

Fig. 4 Time dependence of P-branch maximum gain transitions for v = 5, 10, 15...65 resulting from the time-dependent distributions of Fig. 1.

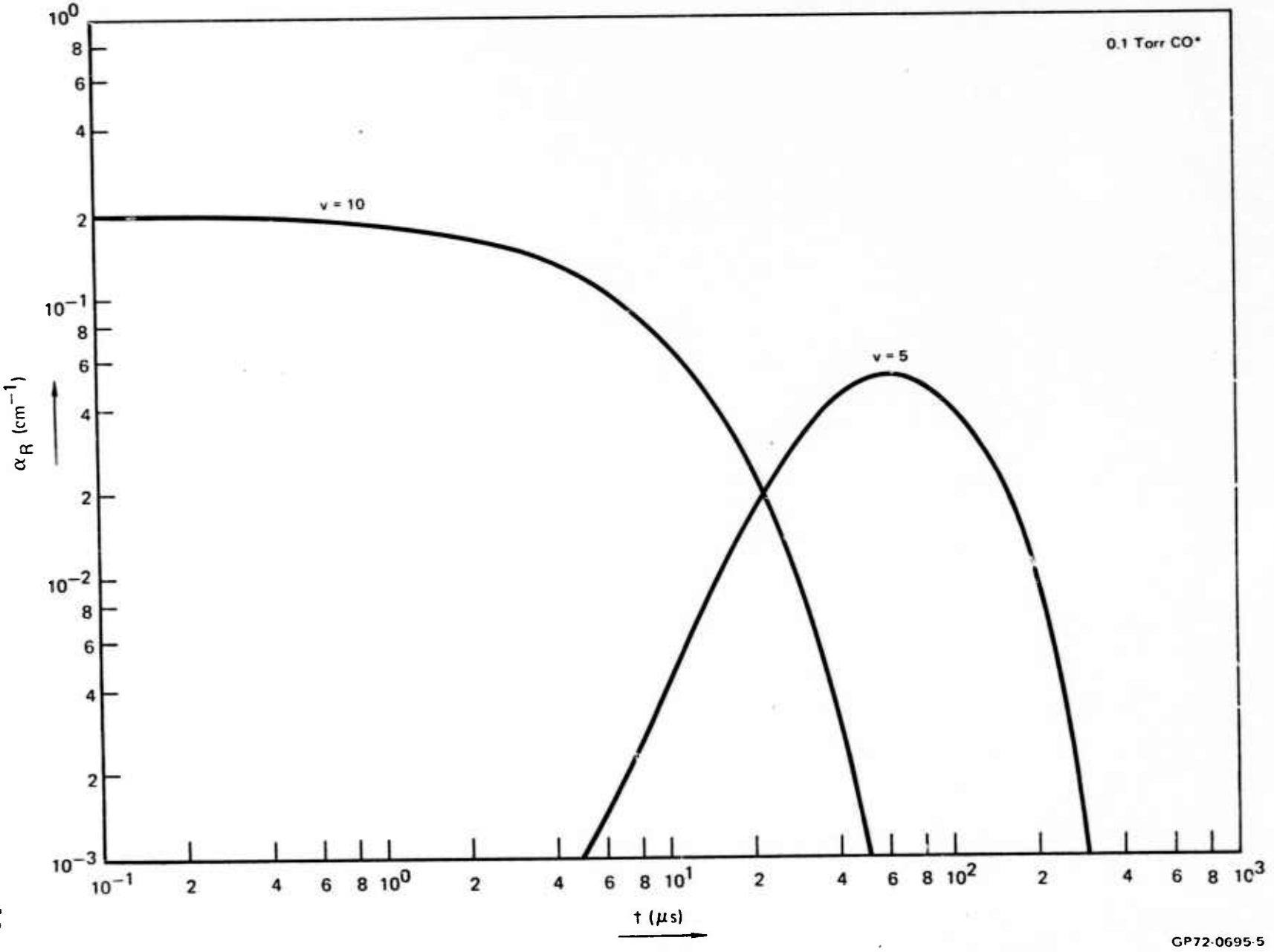

Fig. 5 Time dependence of R-branch maximum gain transitions for v = 5, 10.

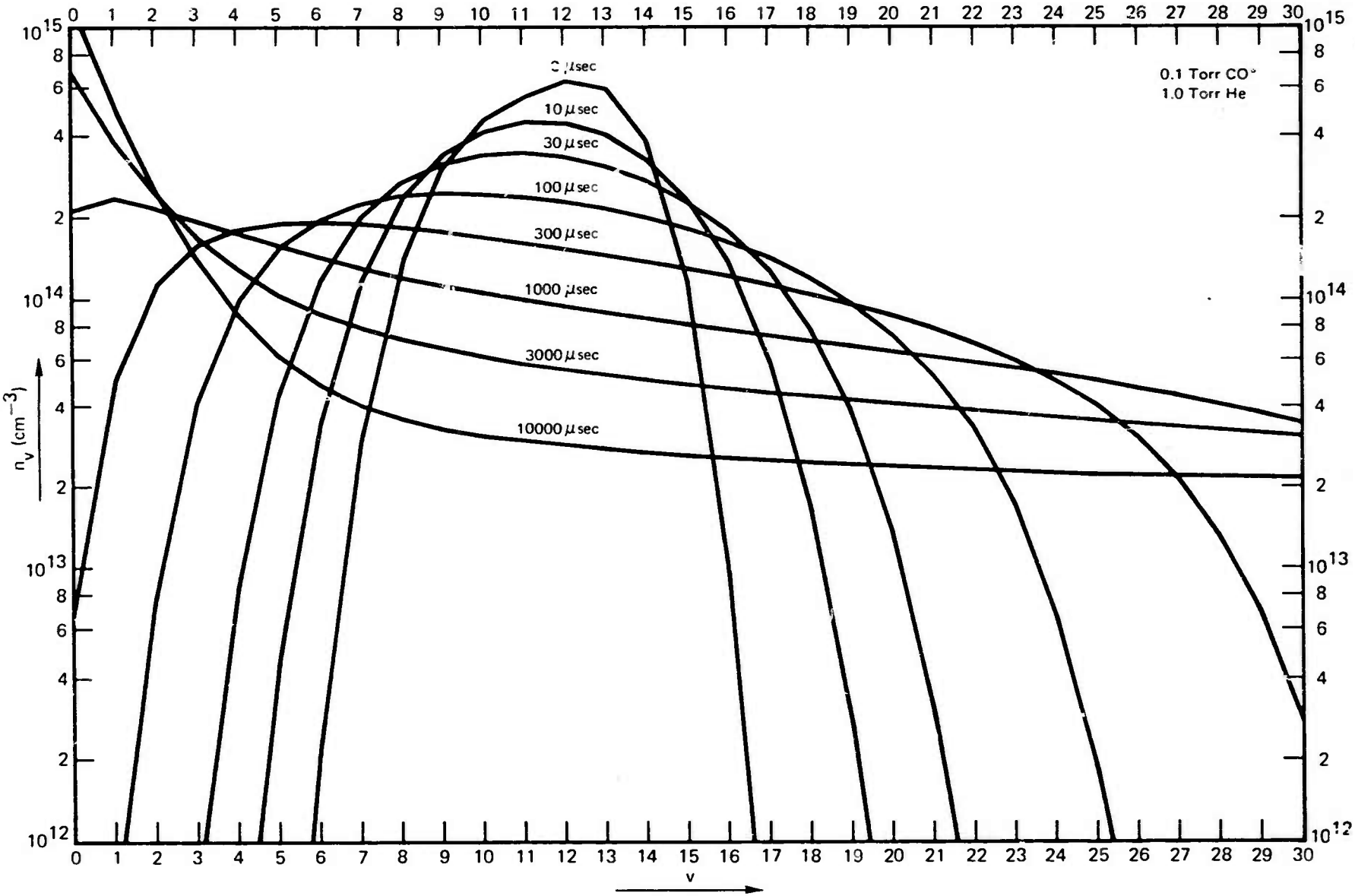

Fig. 6 Relaxation of CO*:He (1:10) at P_{CO*} = 0.1 Torr, P_{He} = 1.0 Torr, T = 300 K.

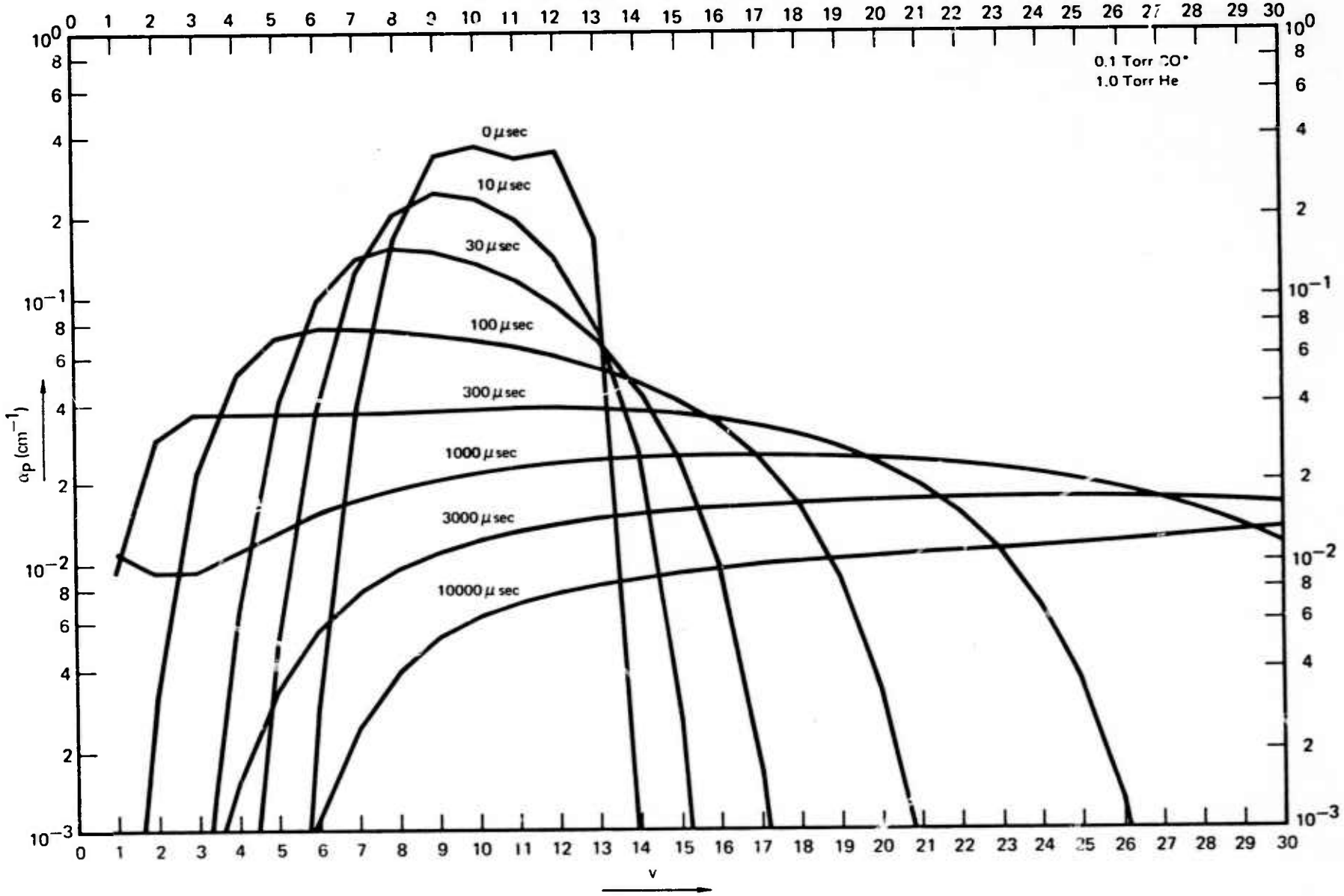

Fig. 7 Maximum P-branch gain coefficients α_p resulting from the time-dependent distributions of Fig. 6.

CO* (CO initially in the chemical distribution) alone. Thus, we conclude that the only effect of He in CO chemical lasers is to act as a temperature-moderating diluent (see below).

Figures 8-10 are the results of the $CO^*:O_2$ (1:10) calculation. The energy separation of the v = 1 to v = 0 states of O_2 is 1556.2 cm^{-1}, which will be nearly resonant with $\Delta v = 1$ CO transitions at v = 24. The V-V transfer probability for the collisions of Eq. (4) thus goes through a maximum with respect to v at v = 24. Therefore, a large excess of O_2 with CO* will act as a barrier to V-V pumping of CO population beyond v = 24. Figure 8 shows this effect quite clearly at times of 1000 μsec or longer, where with O_2 the populations in levels $v \geq 21$ are progressively lower than the case with only CO*. The CO P-branch gain coefficients for $v \leq 20$ are larger by typically 35% at relatively long times ($\sim$ 3000 μsec at 0.1 Torr CO*, 1.0 Torr O_2) because of suppression of upward V-V pumping by O_2. Therefore, with $CO^*:O_2$ ratios of 1:10 or more, the collisional effects of O_2 in the CO chemical laser prevent upward V-V pumping of CO beyond levels of about v = 20.

Figures 11-15 concern the case of "cold" CO and CO*. We have observed in CO chemical lasers that the addition of vibrationally cold CO increases the output power typically by a factor of 2.[9] In CO pulsed electric discharge lasers, the differential relaxation effect of "cold" CO is the mechanism which produces inversion.[10] As shown in Fig. 11, this differential relaxation of the CO* distribution tends to increase the inversion ratios for $v \geq 4$. At the same time the magnitudes of all of the excited populations decrease

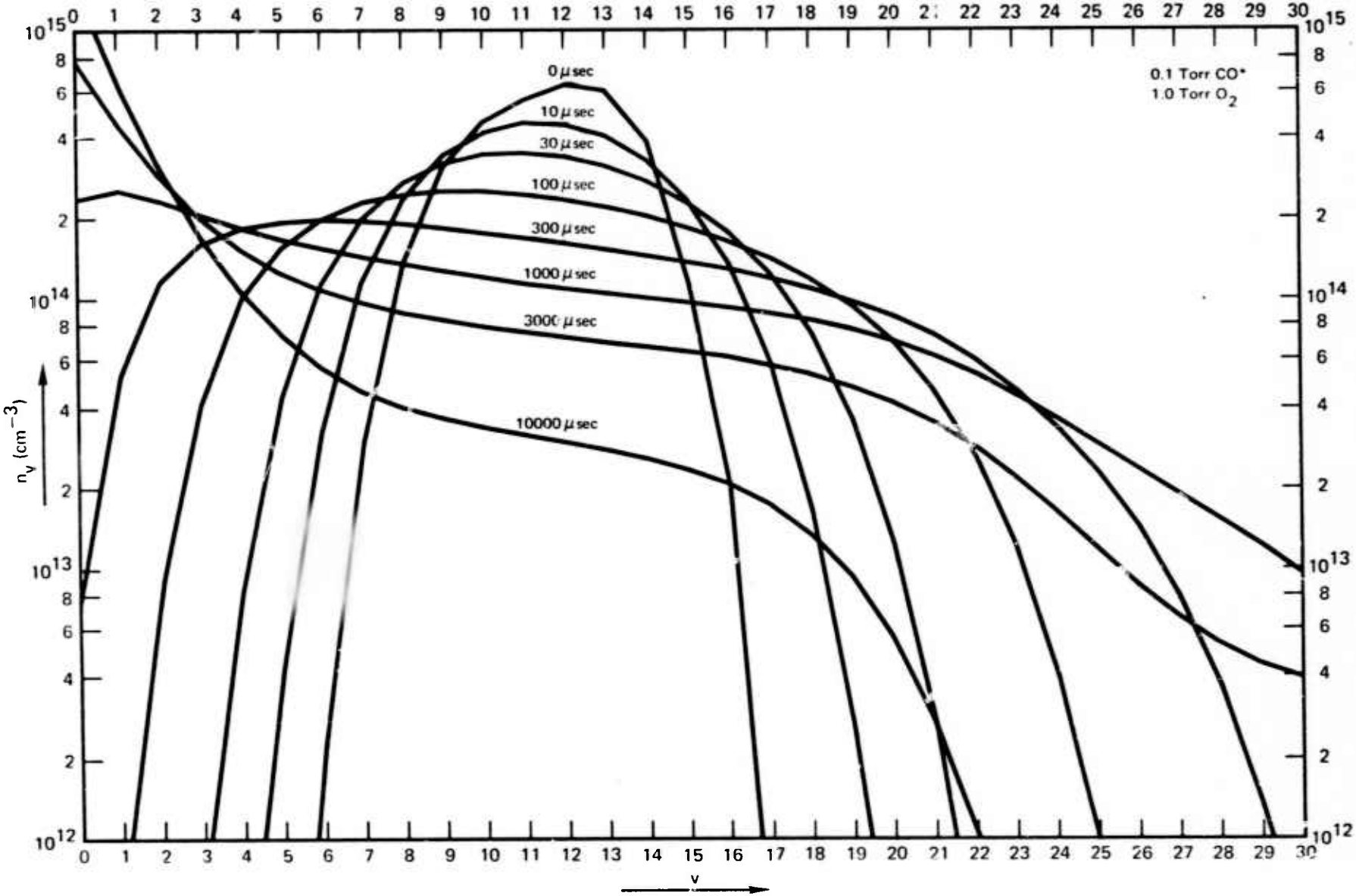

Fig. 8 Relaxation of CO*:O_2 (1:10) at P_{CO*} = 0.1 Torr, P_{O_2} = 1.0 Torr, T = 300 K.

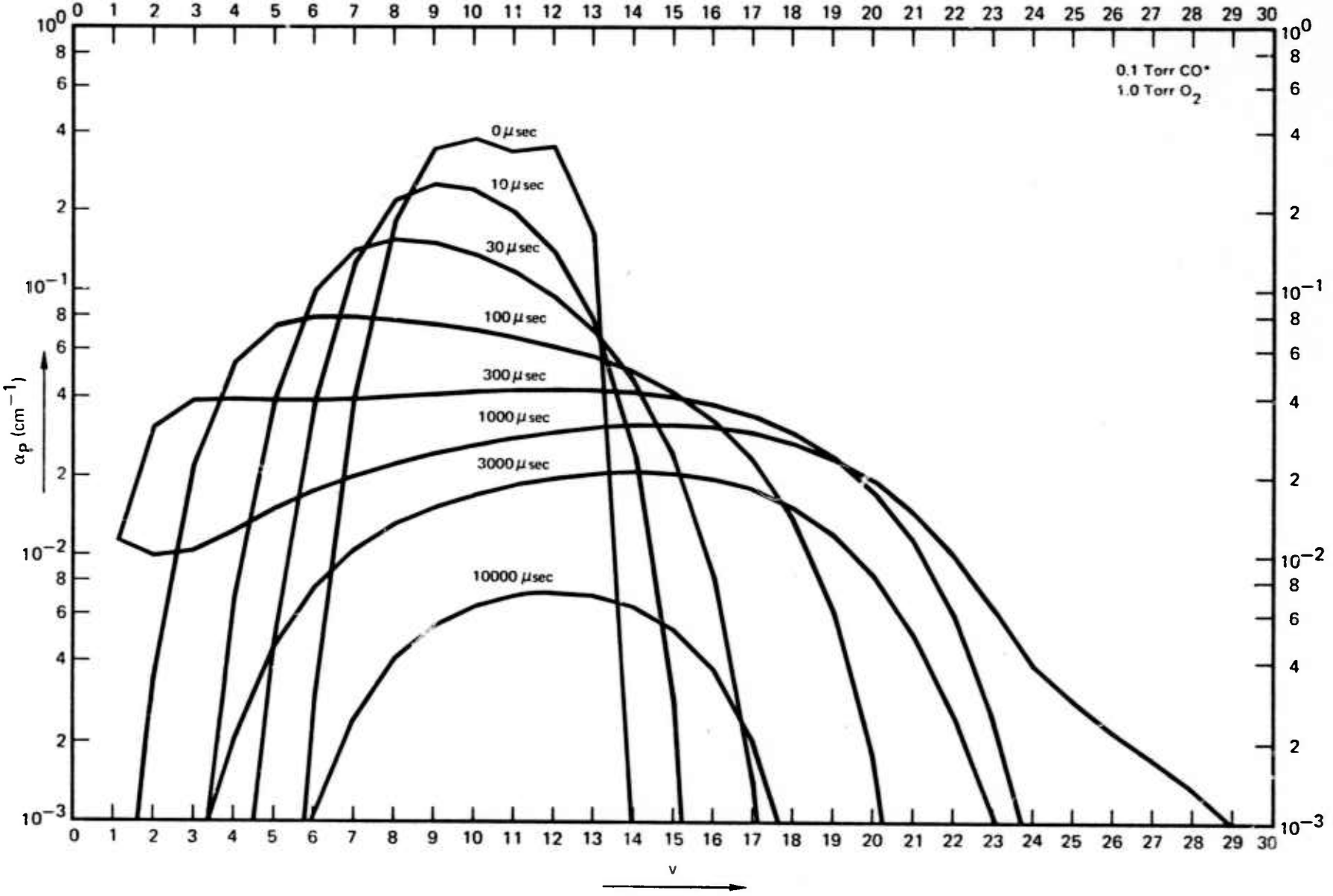

Fig. 9 Maximum P-branch gain coefficients α_p resulting from the time-dependent distributions of Fig. 8.

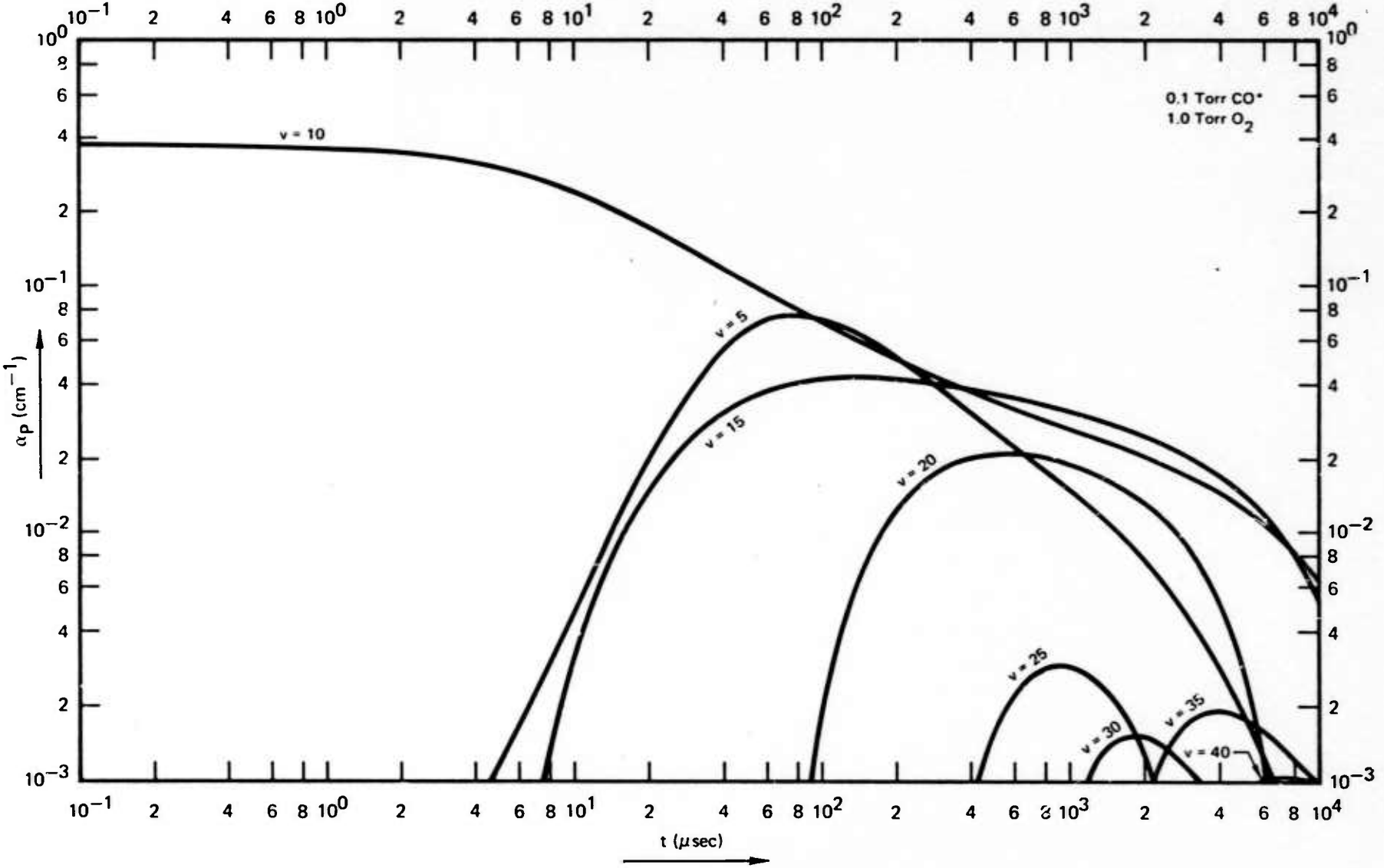

Fig. 10 Time dependence of P-branch gain coefficients for the relaxation of $CO^*:O_2$.

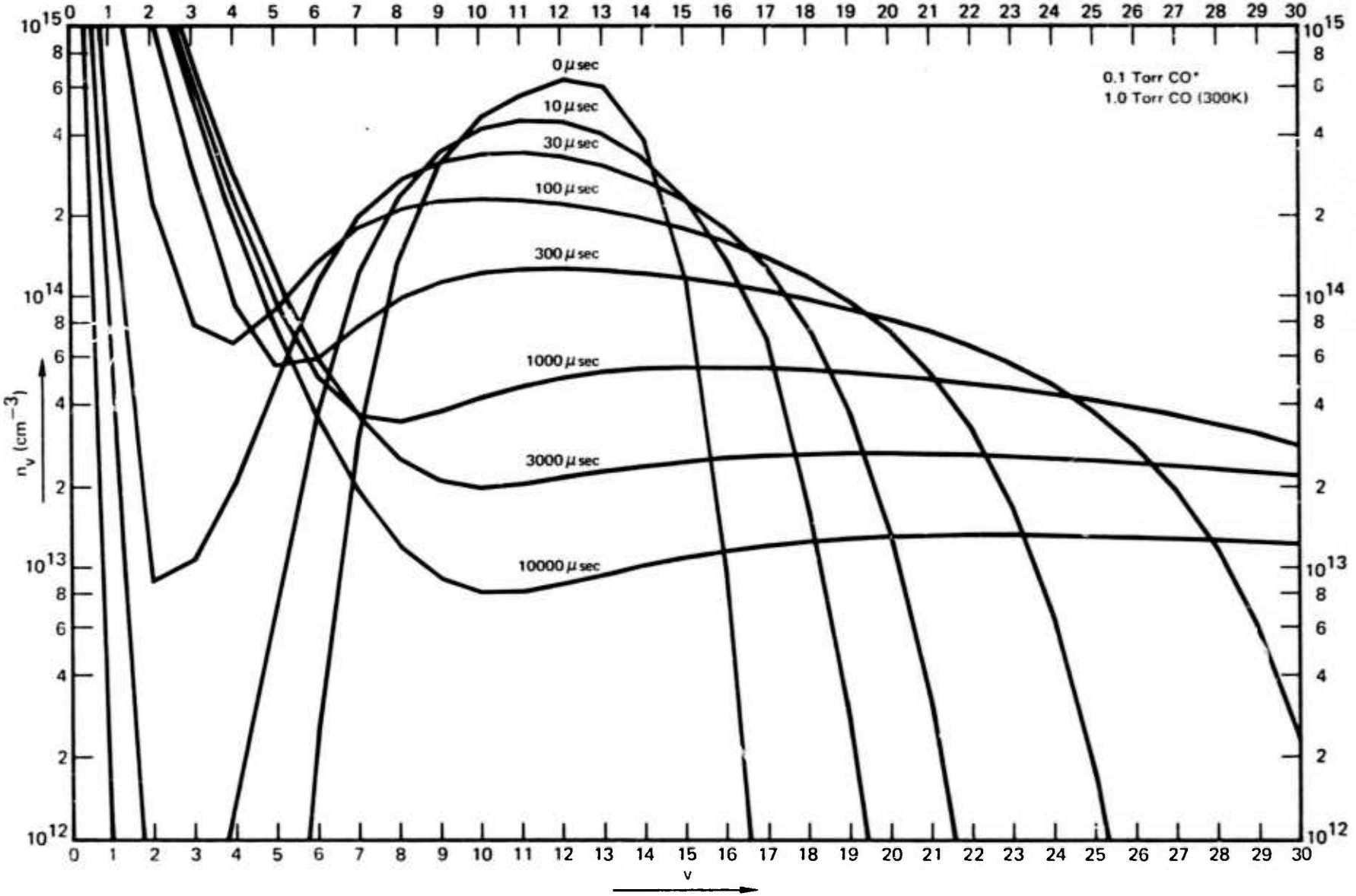

Fig. 11 Relaxation of CO*:CO (300 K) 1:10.

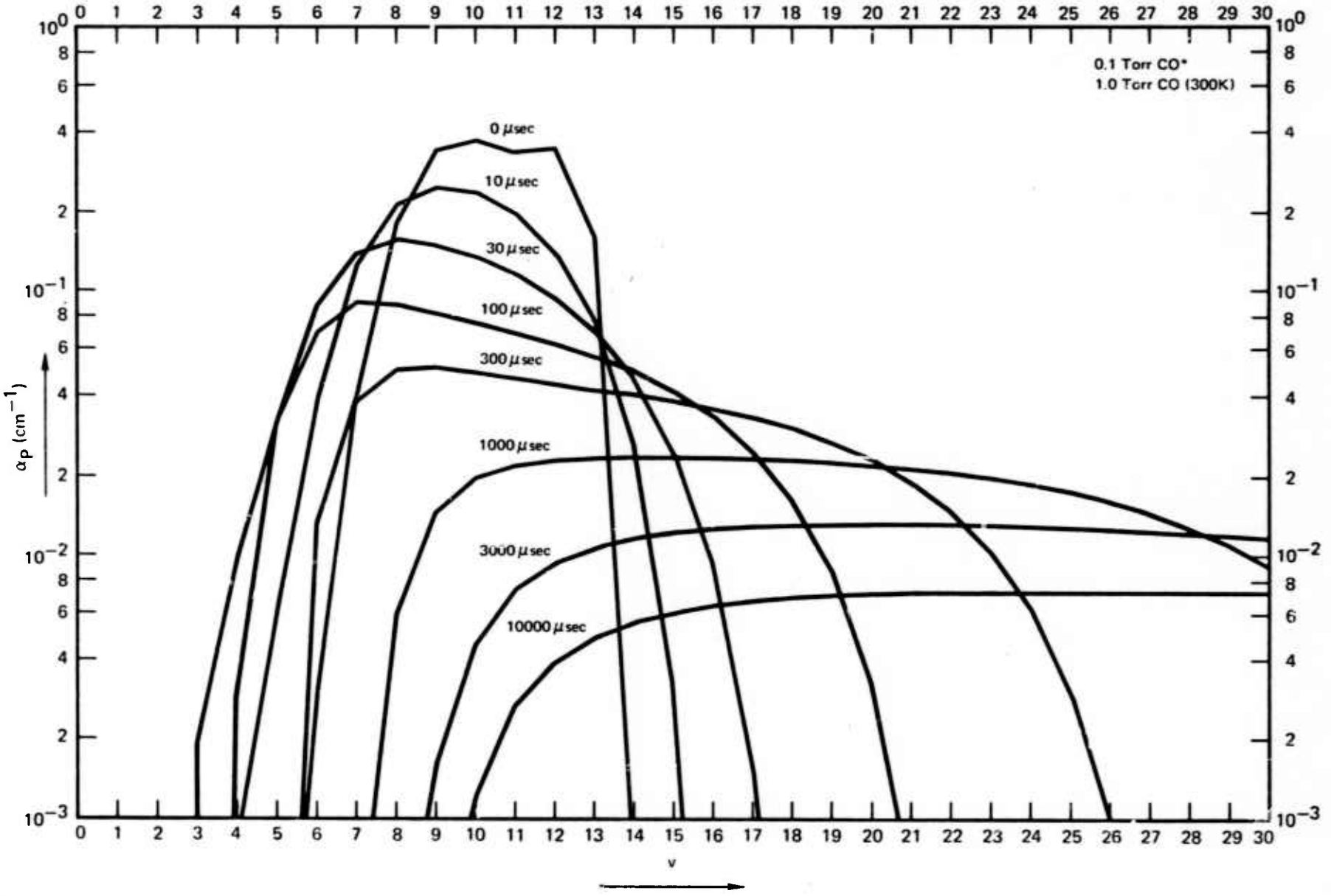

Fig. 12 Maximum P-branch gain coefficients from Fig. 11.

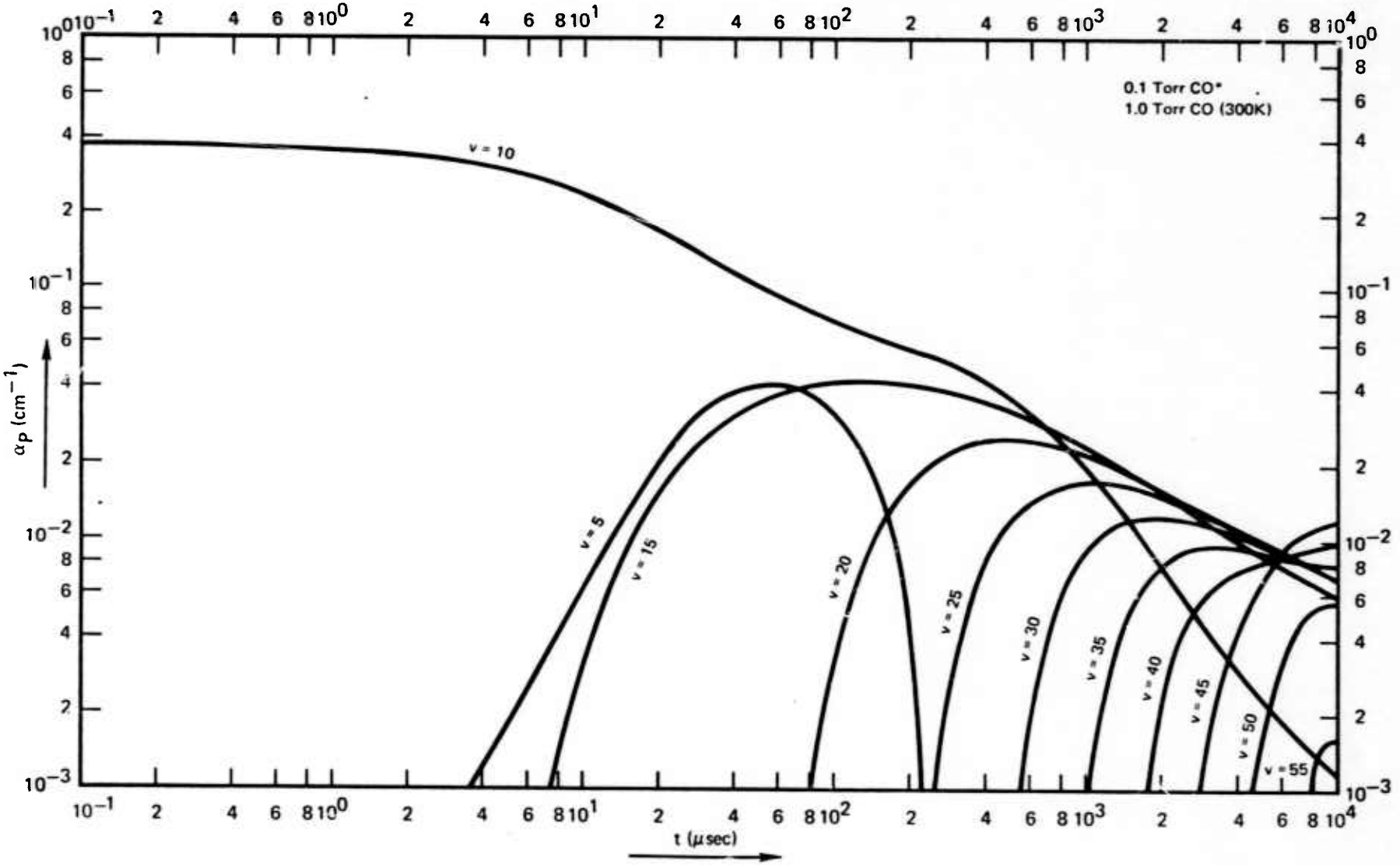

Fig. 13 Time dependence of P-branch gain coefficients from Fig. 11.

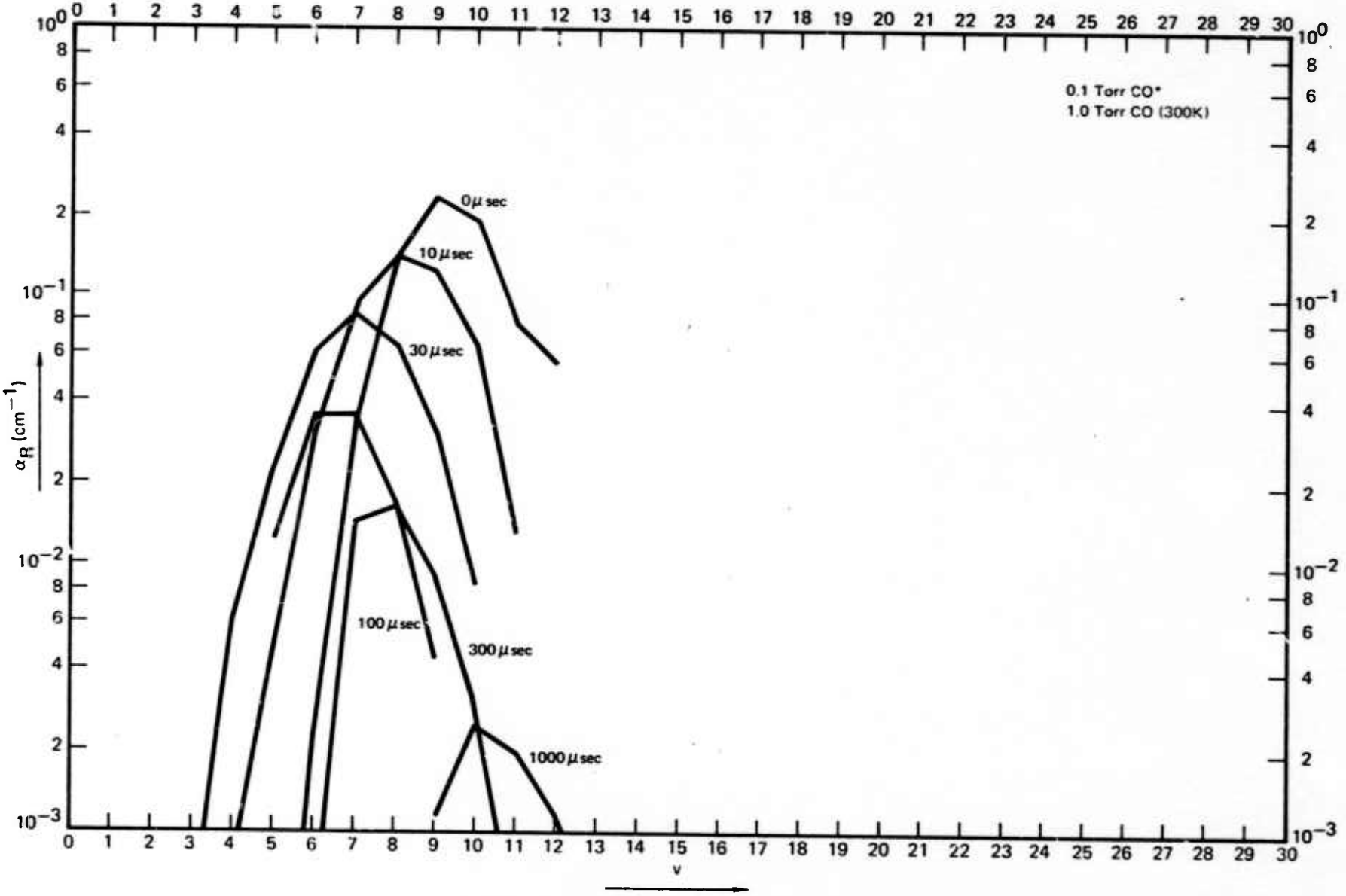

Fig. 14 Maximum R-branch gain coefficients from Fig. 11.

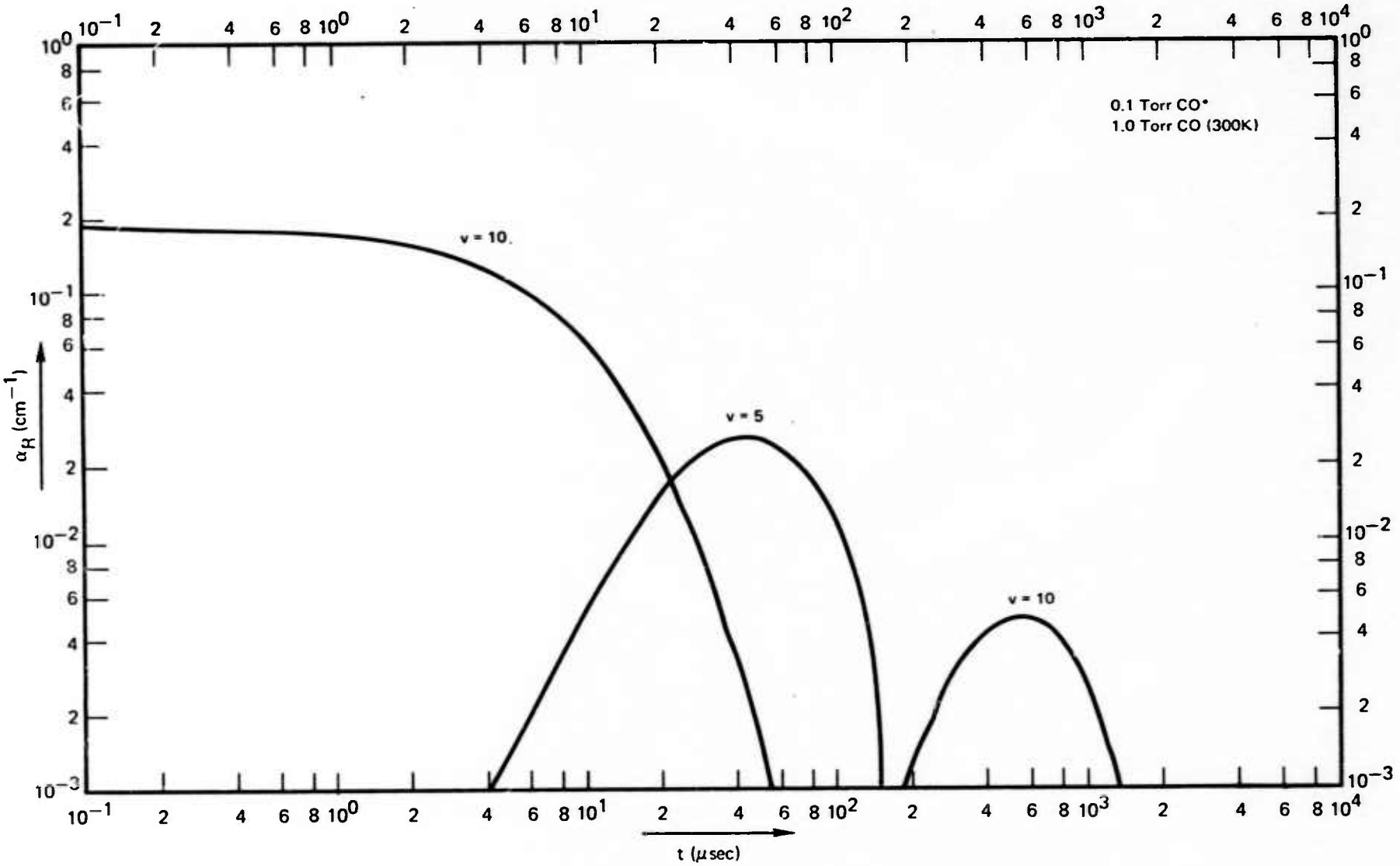

Fig. 15 Time dependence of R-branch gain coefficients from Fig. 11.

more rapidly due to the predominance of the de-exciting collisions,

$$CO(v) + CO(0) \rightarrow CO(v - 1) + CO(1). \qquad (5)$$

The result is a dip in the population distribution which decreases in magnitude and propagates toward high v as the relaxation progresses. In Fig. 11 the minimum of this dip can be seen at v = 4 at 100 μsec, v = 5 at 300 μsec, v = 8 at 1000 μsec, etc. At some given time in the evolution of the CO* distribution, there will be a range of v for which the gain coefficients are larger with "cold" CO than without it. For example at 100 μsec, the α_P are larger at v = 7, 8, 9, 10 in Fig. 12 than in Fig. 2. For v > 10 the α_P are nearly the same for the cases CO* and CO*:CO (1:10), and at v < 7 the "cold" CO decreases α_P. The effects on the R-branch gains can be seen most clearly by comparing Figs. 5 and 15. With CO* alone the chemical distribution predicts large total inversion ratios at t = 0 for the bands from 12 → 11 downwards. As the CO* distribution spreads to lower v by relaxation, the high bands (e.g., 10 → 9) show a monotonic decrease in α_R. Lower bands (e.g., 5 → 4) rise to a maximum and then decrease, since the magnitudes of the initial populations are small. With the addition of "cold" CO, the differential relaxation tends to inhibit relaxation away from total inversion. This can be seen in Fig. 15 where the 10 → 9 α_R comes back to a second peak at 500 μsec.

Figure 16 shows plots of the decay of α^P_{10} (the maximum P-branch gain on the v = 10 → v = 9 transition) for the cases mentioned. The choice of coordinates in this figure is governed by the linear

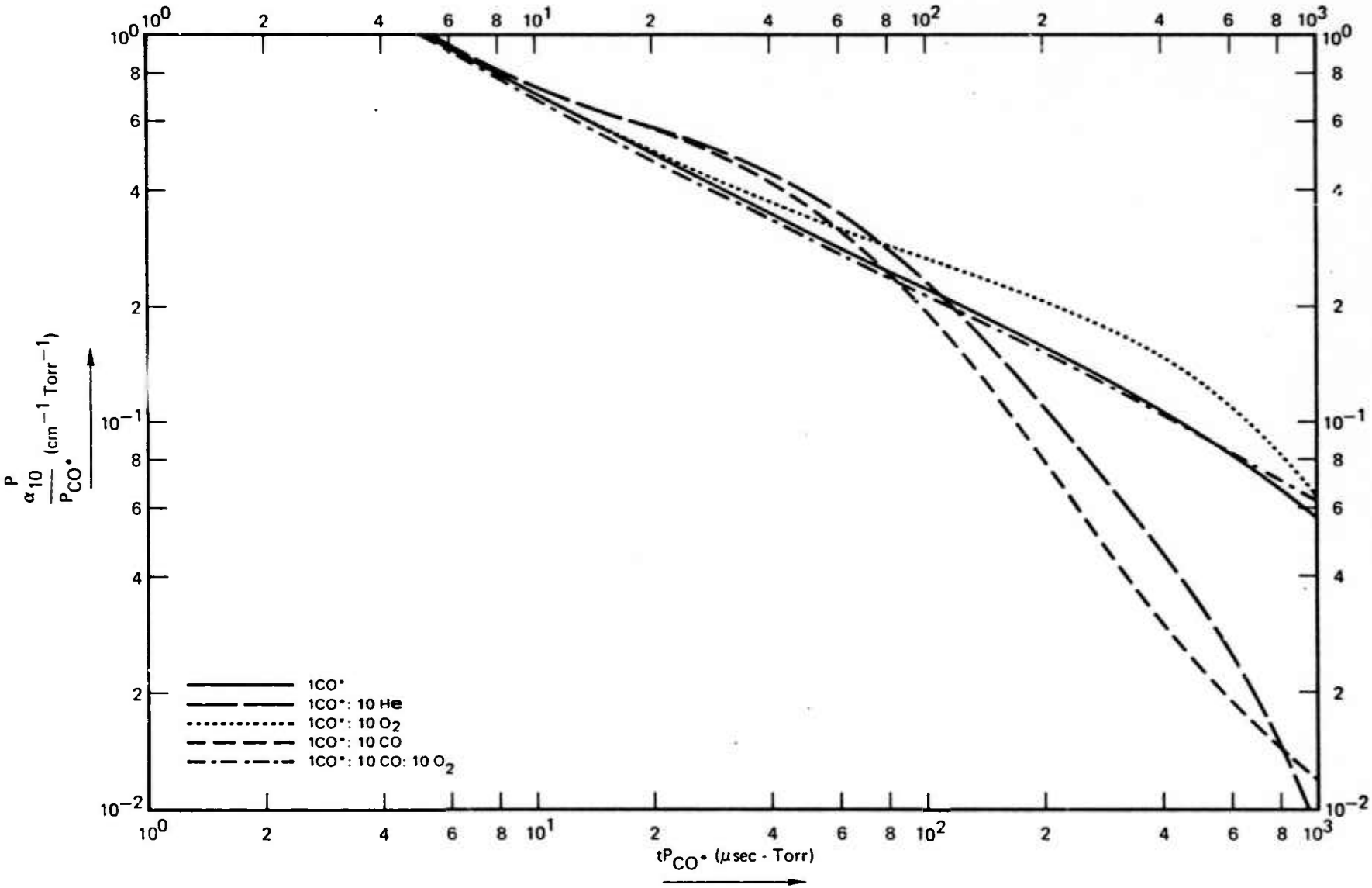

Fig. 16 Summary of CO*:M relaxation (1:10) M = He, O_2, CO (300 K), and CO (300 K) + O_2. Maximum P-branch gain coefficients for 10 → 9 divided by P_{CO^*} versus the product tP_{CO^*}.

dependence of gains on the density of excited-state CO in the region where pressure-broadening is negligible, and by the linear dependence of the logarithmic derivatives of the level populations on gas density in regions where collisional processes dominate the excited state population evolution. The time evolution of α_{10}^{P} may then be determined from Fig. 16 over a reasonably wide range of pressures: 10^{-2} Torr < P_{CO*} < 1 Torr. For tP < 0.5 μsec-Torr, all curves converge on α_{10}^{P}/P_{CO*} = 3.7 $cm^{-1}Torr^{-1}$.

In summary, we have now examined the collisional relaxation effects of those species which will be of major importance in O/CS_2 CO chemical lasers. The predominant effects will certainly be either CO*-CO* relaxation, or CO*-"cold" CO relaxation. Such collision partners as He and O_2 will have only slight effects on the chemically-formed CO.

2.2 Concurrent Fluid Flow, Chemical Kinetics, and Collisional Relaxation of CO*

The program to describe the combined effects of flow, chemistry, and relaxation has been set up to model the flow and geometry of the MDRL chemical laser.[11] The chemistry and relaxation have been treated in a completely general way, and could be adapted to any particular fluid flow situation.

Figure 17 shows a cross section of the reactant flow tubes used in the experimental laser device. Some initial set of species [A] is contained in the main (round) injector at pressure P_A and temperature T_A. This gas is pumped through a slot of width w_A and length L into the cavity region which is assumed to be at pressure P_{cavity}. No pressure gradients are allowed within the cavity region. The initial stream is assumed to be non-reactive. The expansion from the injector interior to the cavity region is assumed to be isentropic, and its temperature, thickness, and flow velocity are computed using this assumption. A specification of the flow rates F_A of all of the species in [A] is given and all species are assumed to behave as ideal gases. For $x < -x_B$ the initial stream quantities are given by

$$T = T_A\left(\frac{P_A}{P_{cavity}}\right)^{1/\bar{g}_A} \tag{6}$$

$$n = \frac{P_{cavity}}{kT} \tag{7}$$

$$v = \left\{\frac{2\bar{g}_A kT}{\bar{m}_A}\left[1-\left(\frac{P_{cavity}}{P_A}\right)^{1/\bar{g}_A}\right]\right\}^{1/2} \tag{8}$$

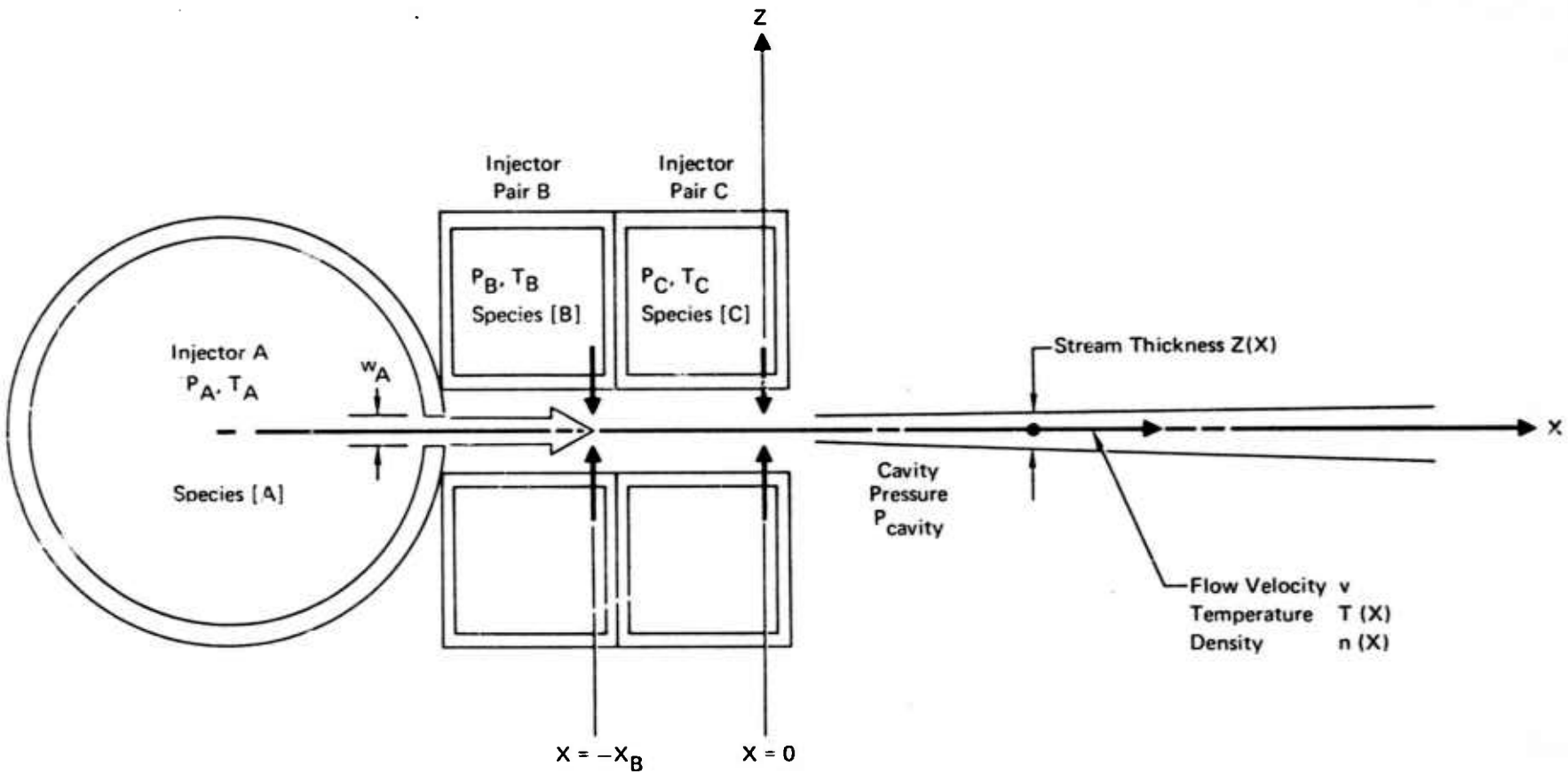

Fig. 17 Cross sectional schematic drawing of the MDRL CO chemical laser injector geometry.

$$z = \frac{F_A}{nvL}, \tag{9}$$

where

$\bar{g}_A$ = 1/2 times the average number of degrees of freedom per particle in the mixture [A], excluding vibration. This represents the heat capacity (excluding vibration) of an ideal gas at constant volume.

$\bar{m}_A$ = average mass per particle in [A]

n = particle number density

v = flow velocity of the initial stream in the x direction

z = thickness of the initial stream (of length L)

F_A = total flow rate of the initial stream (particles/sec).

All of the stream quantities v, z, and T are constant until the initial stream reaches the first injector. This follows from the assumptions:

1. The initial stream is non-reactive, hence no changes in internal energy or chemical species.
2. The gas is assumed inviscid and does not interact with the surrounding gas other than to adjust its internal pressure to p_{cavity}.
3. There are no pressure gradients in the cavity, hence $\frac{dv}{dx} = 0$.

At $x = -x_B$ the initial stream reaches the first transverse injector pair B. The flow of reactants [B] from the injector pair is treated in the same manner as the expansion from the main injector A, with the use of the parameters [B], p_B, T_B, w_B, L, and F_B. The

flow from the injector pair B is assumed to be in the z-direction, so the injectors are properly "transverse" injectors. At $x = -x_B$ the stream quantities are recomputed under the assumption that the combined flows [A] and [B] mix instantly without reaction and come to an internal pressure p_c.

In order to compute the stream quantities at $x = -x_A$, the following conservation laws are used:

Conservation of particles:

$$F = F_A + F_B. \tag{10}$$

Conservation of mass:

$$F\bar{m} = F_A\bar{m}_A + F_B\bar{m}_B. \tag{11}$$

Conservation of number of degrees of freedom:

$$F\bar{g} = F_A\bar{g}_A + F_B\bar{g}_B. \tag{12}$$

Conservation of x-momentum:

$$Fmv\Big|_{x=-x_B} = F_A\bar{m}_A v\Big|_{x<-x_B}. \tag{13}$$

Conservation of energy (at constant pressure):

$$(F_A + F_B)\left(\tfrac{1}{2}\bar{m}v^2 + \bar{g}kT + p\tfrac{1}{n}\right)\Big|_{x=-x_B}$$

$$= F_A\left(\tfrac{1}{2}\bar{m}_A v^2 + \bar{g}_A kT + p\tfrac{1}{n}\right)\Big|_{x<-x_B} \tag{14}$$

$$+ F_B\left(\tfrac{1}{2}\bar{m}_B v^2{}_B + \bar{g}_B kT_B + p\tfrac{1}{n_B}\right).$$

The quantities v_B, $\bar{g}_B$, T_B, and n_B are evaluated for the expanded stream from injector B <u>before</u> mixing with the main stream. v_B is in the z-direction. Thus, at $x = -x_B$ the gases have "mixed"

(for fluid flow purposes) and the new chemical species set [A + B] is known, along with the new values g, m, T, n, v, and z. At $x = -x_B$ the chemical reactions begin, but no instantaneous changes can occur. To model the real situation of finite mixing times, the concentrations of one reaction set, [B], are made available to the chemical reactions with [A] as

$$\frac{dy_i}{dx} = \frac{n_i - y_i}{\ell_{mix}} - \frac{y_i}{z}\frac{dz}{dx} , \qquad (15)$$

where n_i is the density of the i^{th} species in [B], and y_i is that portion of n_i which has been made available to reactant set [A]. The second term arises from stream expansion, z being the stream thickness. The mixing length, ℓ_{mix}, must be furnished as an input parameter. The quantity ℓ_{mix} might be calculated on the basis of some model of the flow and mixing situation (such as diffusive mixing), or it might be chosen as an experimental estimate.

The chemical kinetics have been limited to three reactions since collisional effects on CO are to be allowed with all reactant and product species. In addition, there is evidence that the reactions below are a fairly complete description of $O/O_2/CS_2$ chemistry at temperatures below 500 K:[7]

$$O + CS_2 \xrightarrow{k_{16}} CS + SO - 30 \text{ kcal/mol} \qquad (16)$$

$$k_{16} = (1.07 \times 10^{-10})\, e^{-664.67\, hc/kT} \quad [12]$$

$$O + CS \xrightarrow{k_{17}} CO^* + S - 75 \text{ kcal/mol} \tag{17}$$

$$k_{17} = (4.20 \times 10^{-10})_e^{-709.01\ hc/kT},\ ^{13,14}$$

and

$$S + O_2 \xrightarrow{k_{18}} SO + O - 6 \text{ kcal/mol} \tag{18}$$

$$k_{18} = (2.00 \times 10^{-12})_e^{-0.0\ hc/kT}.\ ^{15}$$

The rates given above are for unit species densities, and the activation energies are in units of cm^{-1} $molecule^{-1}$. References refer to the sources for the rate constants; for the O + CS reaction, an activation energy was deduced from a fit to rate constants at 1100 K[14] and 300 K.[13]

To calculate stream properties at $x > -x_\beta$ the chemical kinetics must be included since the chemical species are changing and the reactions release heat. As before, the stream is allowed to expand or contract so that its internal pressure is p_{cavity}. Let the ℓ^{th} reaction be described by a rate k_ℓ per unit mass, energy release ε_ℓ, and $r_{i\ell}$ the number of particles of species i created or destroyed in each elementary step of the reaction. Then the differential equation for the temperature of the stream is

$$dT = \frac{\bar{m}}{\bar{g}k}\left[\frac{1}{v}\sum_\ell \varepsilon_\ell k_\ell dx - d\tilde{Q}_{rad} - \frac{kT}{\bar{m}z}\,dz\right.$$

$$\left. - d\tilde{U}_v - \frac{kT}{v}\sum_i c_i \sum_\ell r_{i\ell} k_\ell dx\right], \tag{19}$$

where

$\tilde{Q}_{rad}$ = net energy loss through radiative processes per unit mass

$\tilde{U}_v$ = energy stored in vibration per unit mass (only CO)

k = Boltzmann constant.

The stream thickness z is calculated from the differential equation

$$dz = \frac{\bar{m}z}{v(\bar{g}+1)kT}\left[\sum_{\ell}\varepsilon_{\ell}k_{\ell}dx - vd\tilde{Q}_{rad} - vd\tilde{U}_v - kT\sum_{i}(g_i - \bar{g})\sum_{\ell} r_{i\ell}k_{\ell}dx\right]. \quad (20)$$

Between the first transverse injector pair B and the second transverse injector pair C, the stream quantities T and z are calculated from Eqs. (19) and (20), the flow velocity is constant after the discontinuity at $x = -x_B$, and the chemical species are calculated from the rate equations described by the reaction steps (16), (17), and (18).

After the first injection point $x = -x_B$, reaction 17 begins to form CO*. The initial populations of excited states are usually taken to be zero, however, the program also allows for an initial Boltzmann distribution at temperature T. The probability of formation by reaction 17 into each excited state v is the normalized initial distribution of Fig. 1.[6] As in the relaxation calculations the distribution of CO* is calculated by integrating the master equations. Both V-T and V-V collisional energy exchange processes are allowed for <u>each</u> chemical species existing in the set of reactions 16, 17, and 18.

For the V-V processes the following collisions are considered:

$$CO(v) + CO(v') \rightarrow CO(v \pm 1) + CO(v' \mp 1) \quad (21)$$

$$CO(v) + CS_2(00^00) \rightarrow CO(v - 1) + CS_2(00^01) \quad (22)$$

$$CO(v) + CS(v = 0) \rightarrow CO(v - 1) + CS(v = 1) \quad (23)$$

$$CO(v) + SO(v = 0) \rightarrow CO(v - 1) + SO(v = 1) \quad (24)$$

$$CO(v) + O_2(v = 0) \rightarrow CO(v - 1) + O_2(v = 1). \quad (25)$$

All of the species except CO are assumed to be entirely in their ground vibrational states, so that the reverse processes of Eqs. (22) - (25) are not allowed. The CO-CO and CO-O_2 V-V transfer probabilities have been discussed above in the relaxation calculations. The CO-CS_2, CO-CS, and CO-SO collisions were treated using only short range forces as was done for CO-O_2.

For the V-T processes, the general event is

$$CO(v) + M \rightarrow CO(v - 1) + M, \quad (26)$$

where M = CO, CS_2, CS, SO, O_2, He, and S. All of these V-T transition probabilities have been computed using the standard SSH theory. In the cases CO-He and CO-O_2 the computed results were scaled to match experimental data.

There is one further difference between the calculations with chemical kinetics and the relaxation calculations. Inasmuch as the fluid flow evolves at constant pressure, and therefore the gas kinetic temperature is variable, the V-V and V-T probabilities are allowed to vary with temperature. This temperature dependence is described parametrically in the form:

$$P(T) = \exp(a + bT^{-1/3} + cT^{-1}), \tag{27}$$

where the parameters a, b, and c are chosen to fit the computed probabilities at 100 K, 300 K, and 700 K.

2.3 Results

The kinetics program described above has been run with two cases chosen to reproduce as closely as possible the experimental conditions of the MDRL CO chemical laser device. The "standard conditions" described below have been used to obtain experimental data reported in the First Quarterly Progress Report.[1] All of the conditions necessary for these two runs of the program are listed in Table I, with footnotes as additional explanation.

Turning first to the fluid flow and chemical kinetics, Fig. 18 shows the computed stream thickness, temperature, and flow velocity for Case I. The computed quantities at x = 0.6 cm are of interest since the cavity optical axis is located at that position. The only quantity of these three which has been directly measured is the gas temperature. An epoxy-coated thermocouple positioned at x = 0.6 cm showed a temperature rise with the addition of CS_2 to the O, O_2, He stream of 75 K, while the calculated rise is 53 K. This point will be discussed further below; the values of stream thickness and flow velocity are reasonable and agree with our qualitative experimental estimates.

The chemical species densities are shown in Fig. 19. The gas expansion effects are included in these densities; the He density varies from $1.806 \times 10^{17}/cm^3$ at x = -1.2 cm to $1.137 \times 10^{17}/cm^3$ at x = 10.0 cm. In these cases the reactions are operated oxygen atom rich on the basis of our estimated 10% O_2 dissociation, and the CS_2 is more than 90% reacted at x > 3.0 cm. Consequently the CO concentration rises to a steady state value of $2.45 \times 10^{15}/cm^3$,

Table I. Input data for kinetics program[a]

	Case I	Case II
Injector A		
Reactant molar flowrates (mmoles/sec)	$He:O_2:O = 17.7:3.78:0.84$[b]	$He:O_2:O = 17.7:3.78:0.84$[b]
p_A (Torr)	9.4[c]	9.4[c]
T_A (K)	315[d]	315[d]
Injector Pair B		
Reactant molar flowrates (mmoles/sec)	$CS_2 = 0.38$	$CS_2 = 0.38$
p_B (Torr)	11.0[c]	11.0[c]
T_B (K)	300	300
Mixing length (cm)	0.5[e]	0.5[e]
Position	x = -1.2 cm	x = -1.2 cm
Injector Pair C		
Molar flowrate (mmoles/sec)	0.0	CO = 2.3
p_C (Torr)	-	56.0[c]
T_C (K)	-	300
Mixing length (cm)	-	0.5[e]
Position	-	x = 0.0 cm
Cavity Conditions		
p_{cavity} (Torr)	5.85[c]	6.85[c]

[a] See Fig. 17

[b] All molar flowrates are measured values, except [O]. A value for the atomic oxygen flowrate is obtained by assuming 10% dissociation of the net O_2 flow.

[c] Measured value

[d] Measured in A injector

[e] Estimated

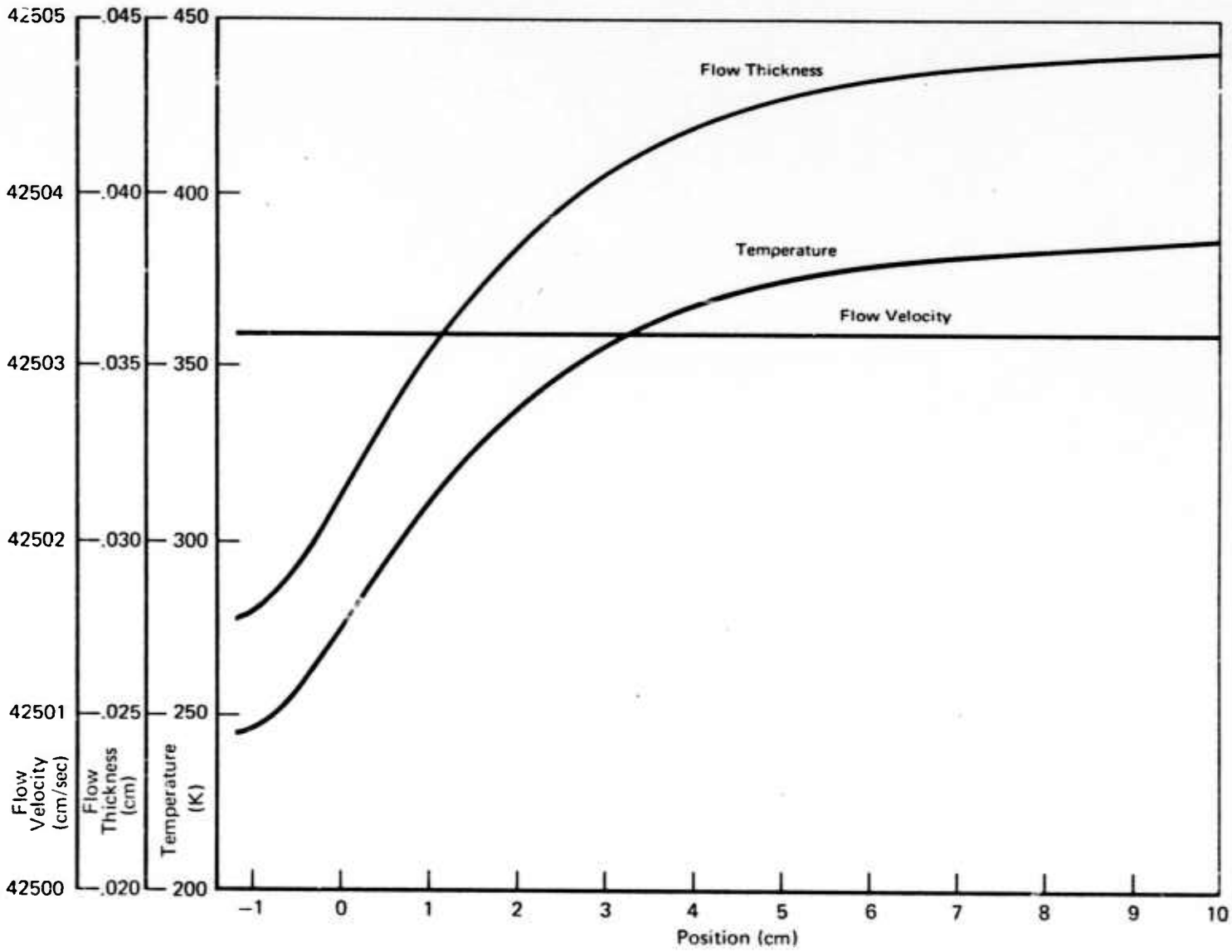

Fig. 18 Computed stream quantities z(x), T(x), and v for Case I.

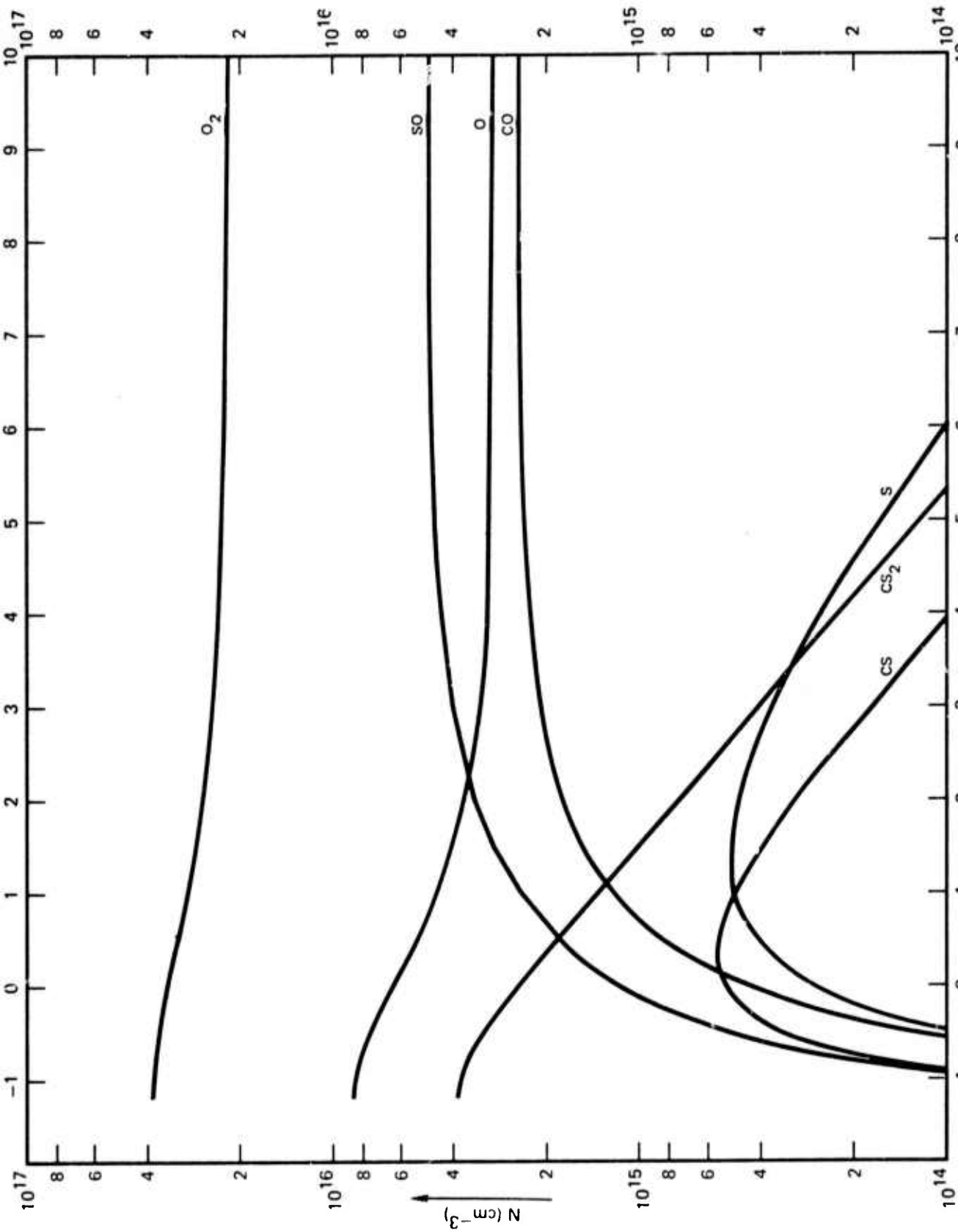

Fig. 19 Chemical species densities as a function of stream position for Case I.

corresponding to a partial pressure of about 0.1 Torr. The difference between the CO and S densities is a measure of the participation of the S + O_2 reaction.

Figures 20 through 24 show the population density and optical gain coefficients for Case I. Since the mixing distance is taken to be 0.5 cm, the initial effect of the reactions is to build up an excited distribution of CO with relatively little relaxation. As Fig. 20 shows, the CO distribution seen by the optical cavity at x = 0.6 cm (or t $\simeq$ 37 μsec) will be close to the CO* distribution. By x $\geq$ 3 cm (t $\gtrsim$ 100 μsec), the CS_2 has been nearly depleted, and the CO distribution begins to broaden by collisional relaxation.

Figures 21 and 22 show the resulting maximum P- and R-branch gains versus v with time (or position) as a parameter. Since these are zero-intensity gain coefficients, the only comparison to be made to experiment is the predicted bands versus those observed.[1,11] Taking the optical cavity losses to be a minimum of 3% in the single line measurements, bands with a value of α greater than 3×10^{-4} cm^{-1} (at x = 0.6 cm) should be seen. From Figs. 21 and 22 the predicted bands are 14 → 13 down to 6 → 5. The observed bands in Table II are 12 → 11 down to 7-6 (for the P-branch). This suggests that the estimated 10% dissociation of O_2 is too high, with the resulting CO density and P-branch gain coefficients too large in magnitude. A more serious difficulty arises with the R-branch gain coefficients of Fig. 24. The maximum α_R on the 9 → 8 band is predicted to be only a factor of 4.4/6.4 lower than α_P at x = 0.6 cm. Similarly, gains of 10^{-2} or larger are predicted for α_R on the 11 → 10 through

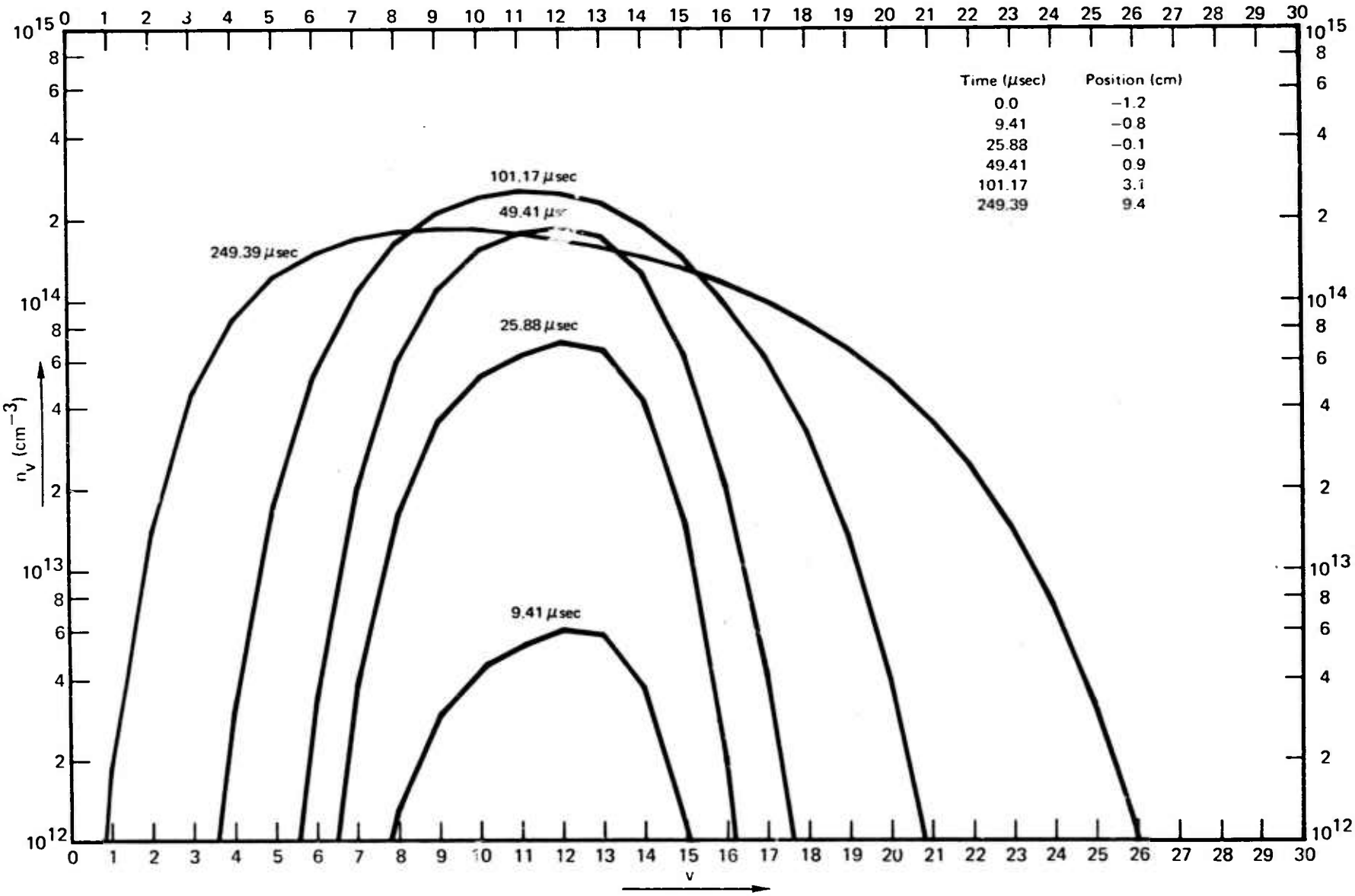

Fig. 20 CO* population distributions for Case I. Equivalent times (after CS_2 injection) and positions are given.

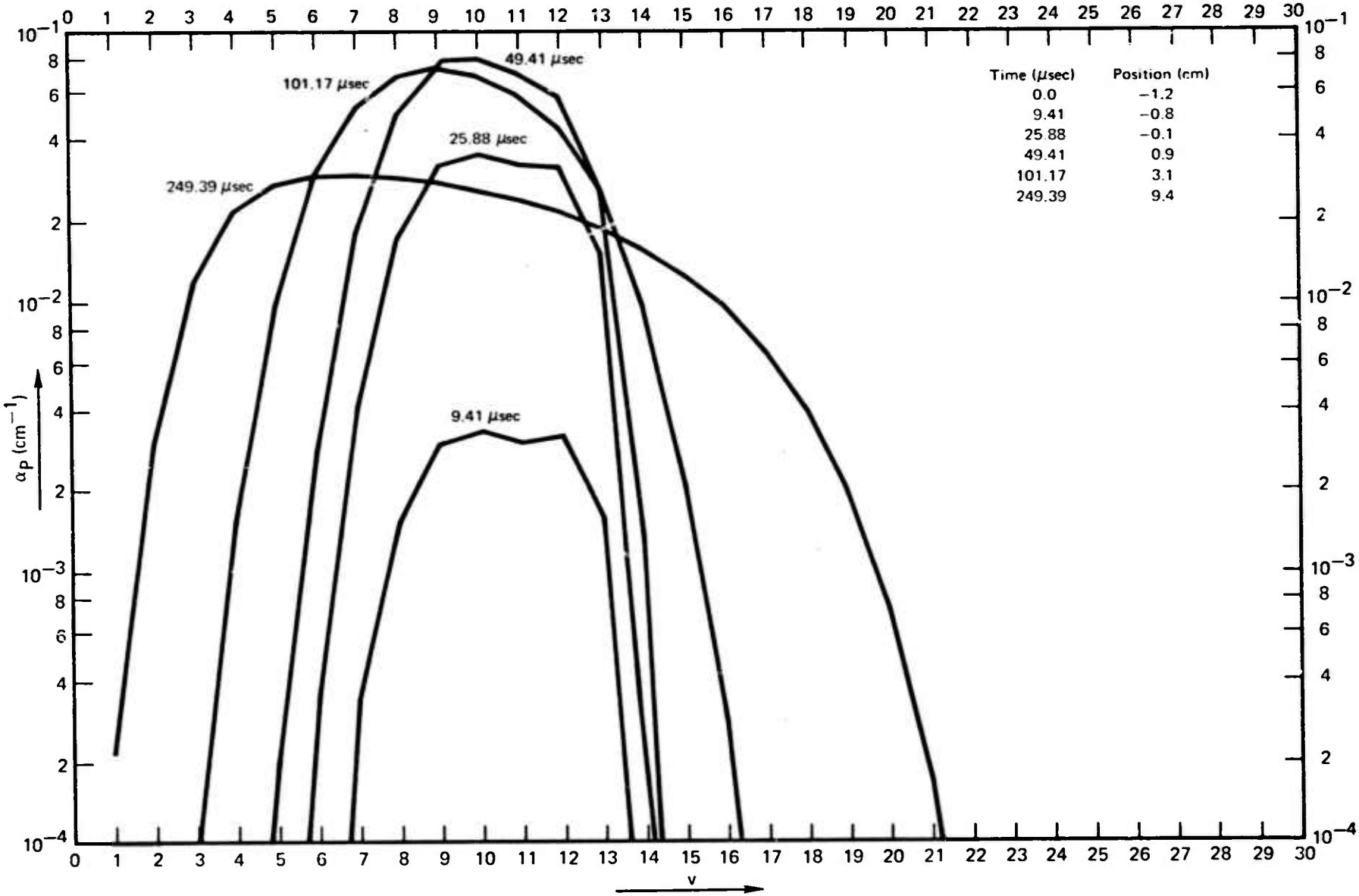

Fig. 21 Maximum P-branch gains resulting from the population distributions of Fig. 20.

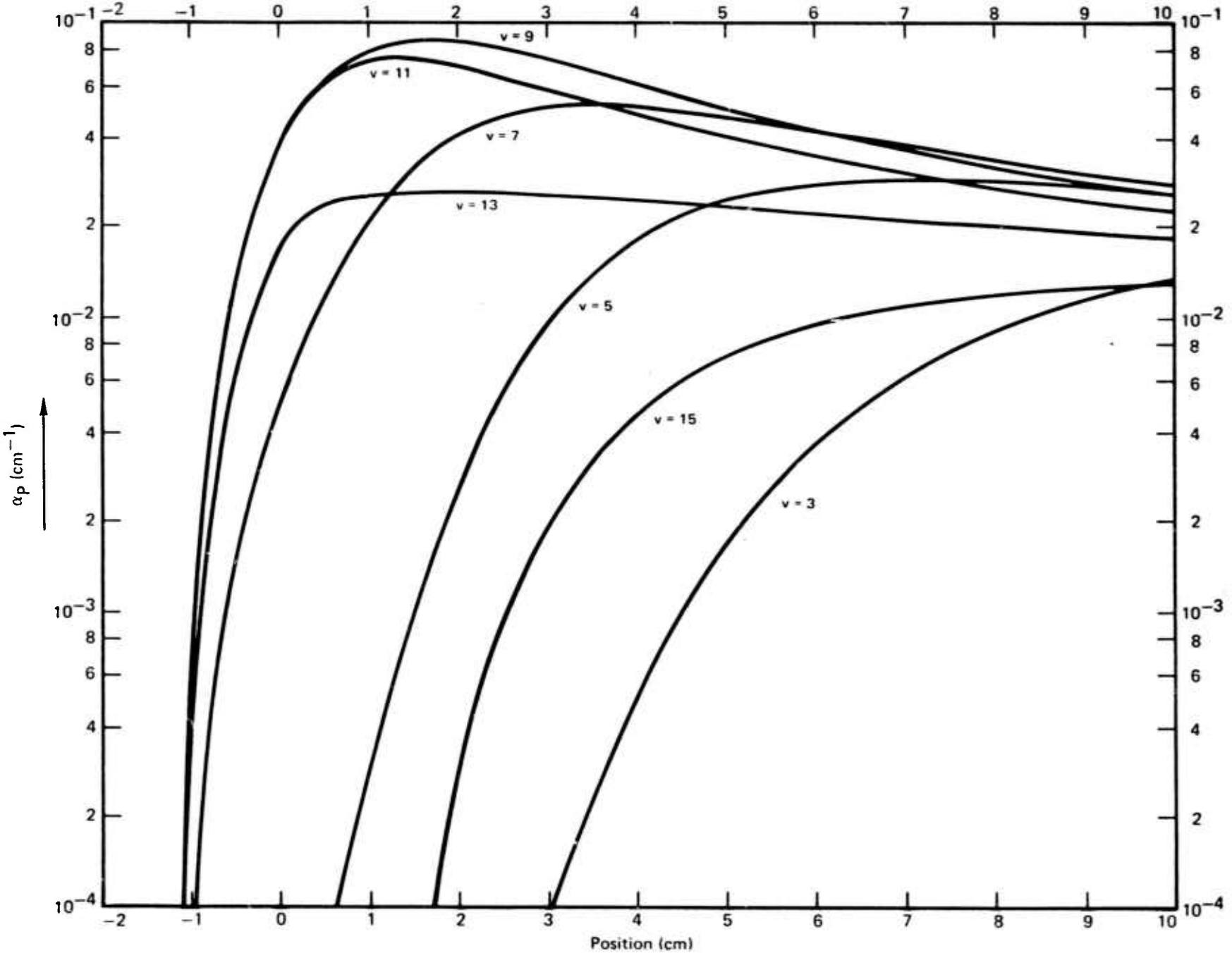

Fig. 22 Maximum P-branch gains versus position from Fig. 20.

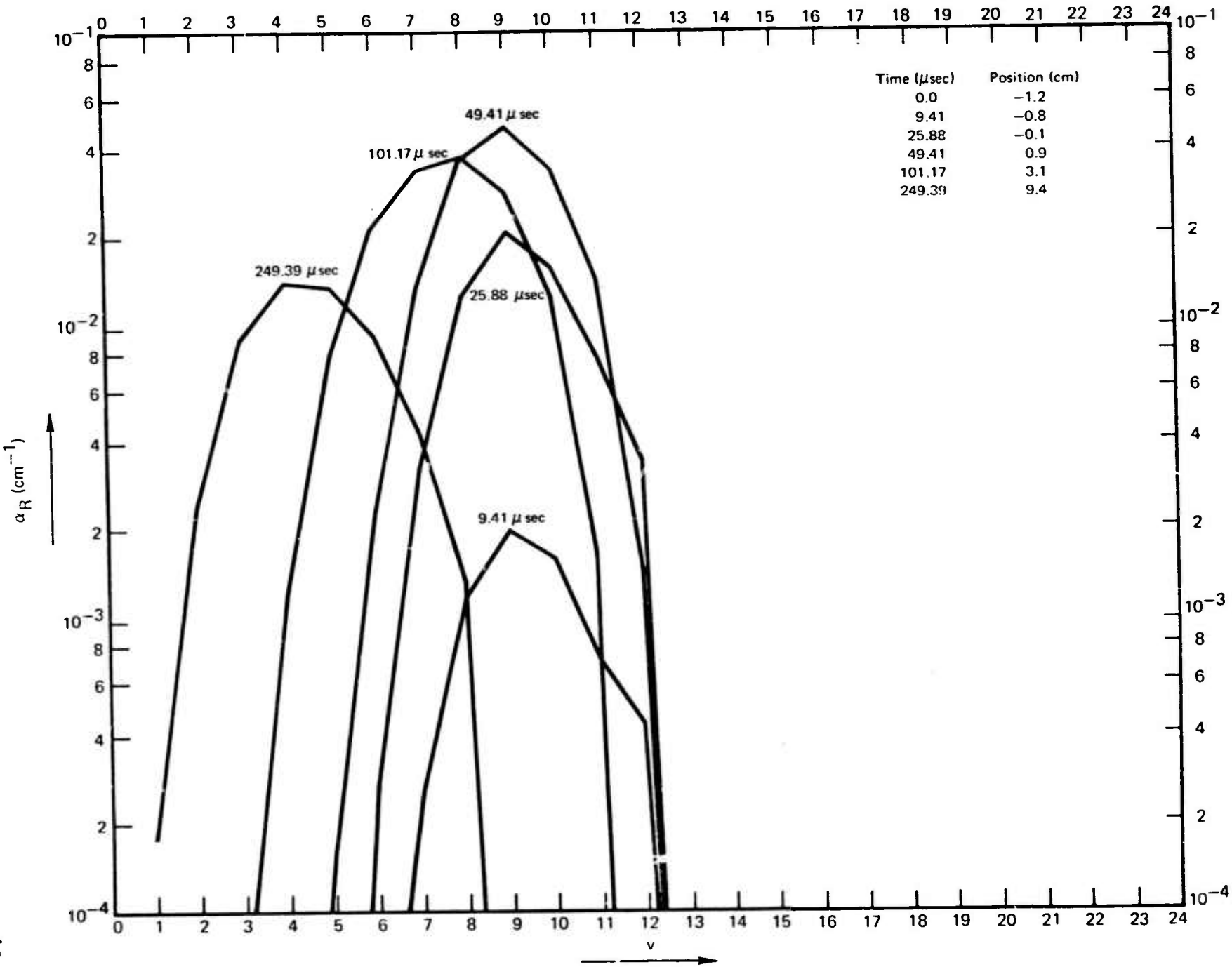

Fig. 23 Maximum R-branch gains from Fig. 20.

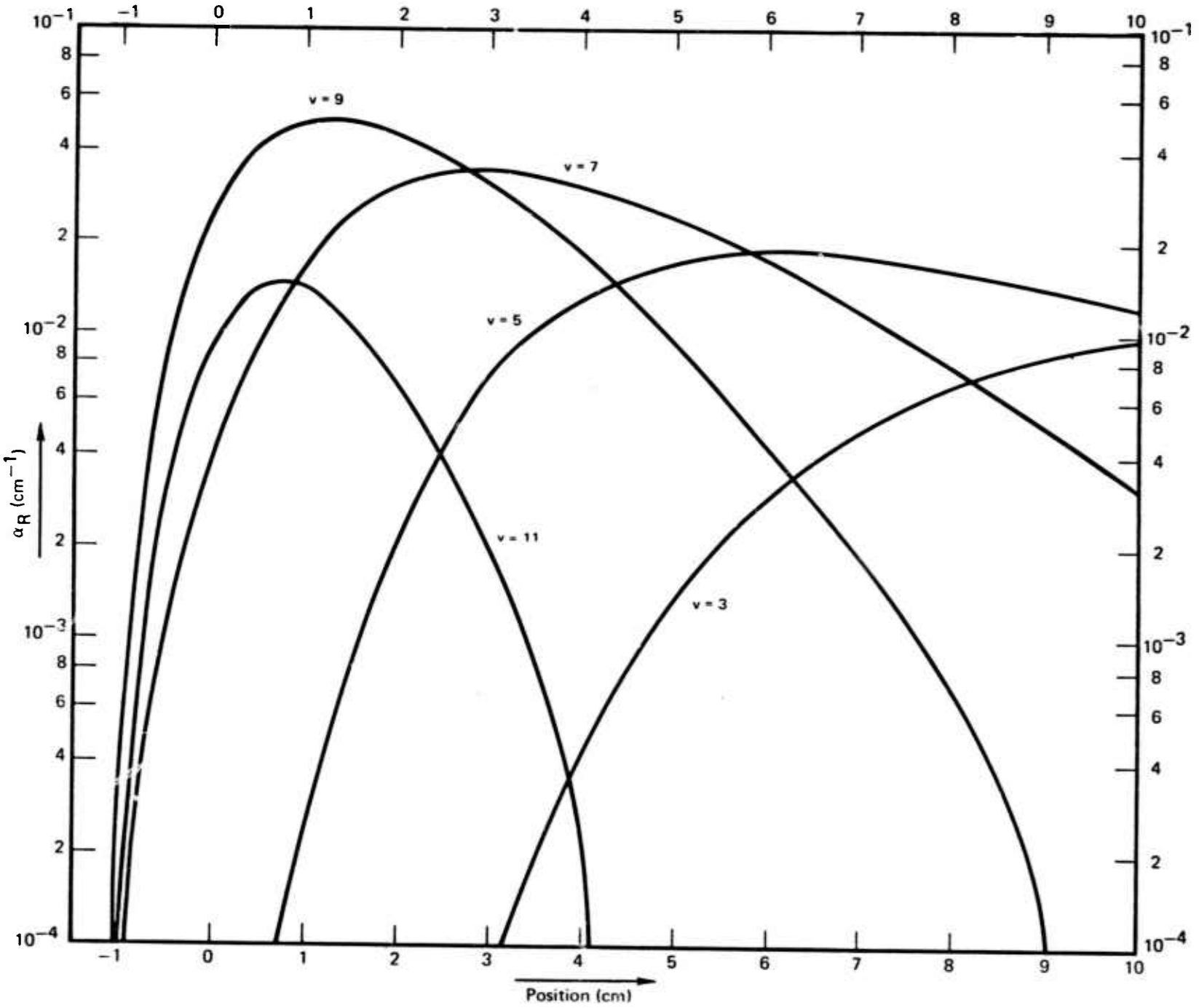

Fig. 24 Maximum R-branch gains versus position from Fig. 20.

Table II. Single line spectra observed in MDRL CO chemical laser with conditions of Case II of Table I.

Band, branch

J	7→6		8→7		9→8		10→9		11→10		12→11	
	R	P	R	P	R	P	R	P	R	P	R	P
0							O					
1				O		O	√	O				
2				√	O	√	√	√	√	O		
3			O	√	√	√	√	√		√		
4			√	√	√	√	√	√		√		
5		O	√	√	√	√	√	√		√		
6		√	√	√	√	√	√	√		√		
7		√	√	√	√	√	√	√		√		
8		√	√	√	√	√	√	√		√		O
9		√	√	√	√	√	√	√		√		√
10		√	√	√	√	√	√	√		√		√
11		√	√	√	√	√	√	√		√		√
12		√	O	√	√	√	√	√		√		√
13		√		√	√	√	O	√		√		√
14		√		√	√	√		√		√		O
15		√		√	√	√		√		√		
16		O		√	O	√		√		√		
17				√		√		√		√		
18				√		√		√		√		
19				√		√		√		√		
20				√		√		√		O		
21				√		√		√				
22				O		O		√				
23								O				
24												
25												

√ = line observed
O = unable to get oscillation

7 → 6 bands. Our experimental observations were that R-branch lines could be seen only with cold CO injection (Case II).[11] A scale change in the CO density (and hence all of the excited CO populations and gain coefficients) will not resolve this discrepancy since the population distribution at x = 0.6 cm is nearly characteristic of the CO* distribution unmodified by relaxation.

Figures 25 through 29 display the populations and gain coefficients for Case II which is identical to Case I except for cold CO injection at x = 0.0 cm. (This injection leads to the discontinuities of the α_P and α_R in Figs. 28 and 29 because of changes in CO* densities and in the pressure-broadened linewidths.) The effects of the cold CO injection are primarily to suppress gain on the low bands at long times ($v < 5$ for $t \geq 250$ sec), and to enhance the gains on higher bands. For example, at x = 0.6 cm, α_R on 7 → 6 is a factor of 2.4 larger with cold CO injection than without.

It is recommended that some refinements be made to this model of the CO chemical laser. The fluid flow description should be modified to include viscous effects which will tend to broaden and slow the gas stream. Additional reaction steps may be added to the chemical kinetics. Perhaps most important, we suspect the CO* distribution of Reference 6 may be in error for $v < 6$. Other work has resulted in a distribution which has substantial formation in the states below v = 6.[16] Changes in the CO* distribution will have profound effects on the stream quantities (through heat release to translation by the O + CS reaction), and on the optical properties of the CO medium. The CO* distribution may resolve the discrepancy discussed above in the P- and R-branch gain coefficients of Case I.

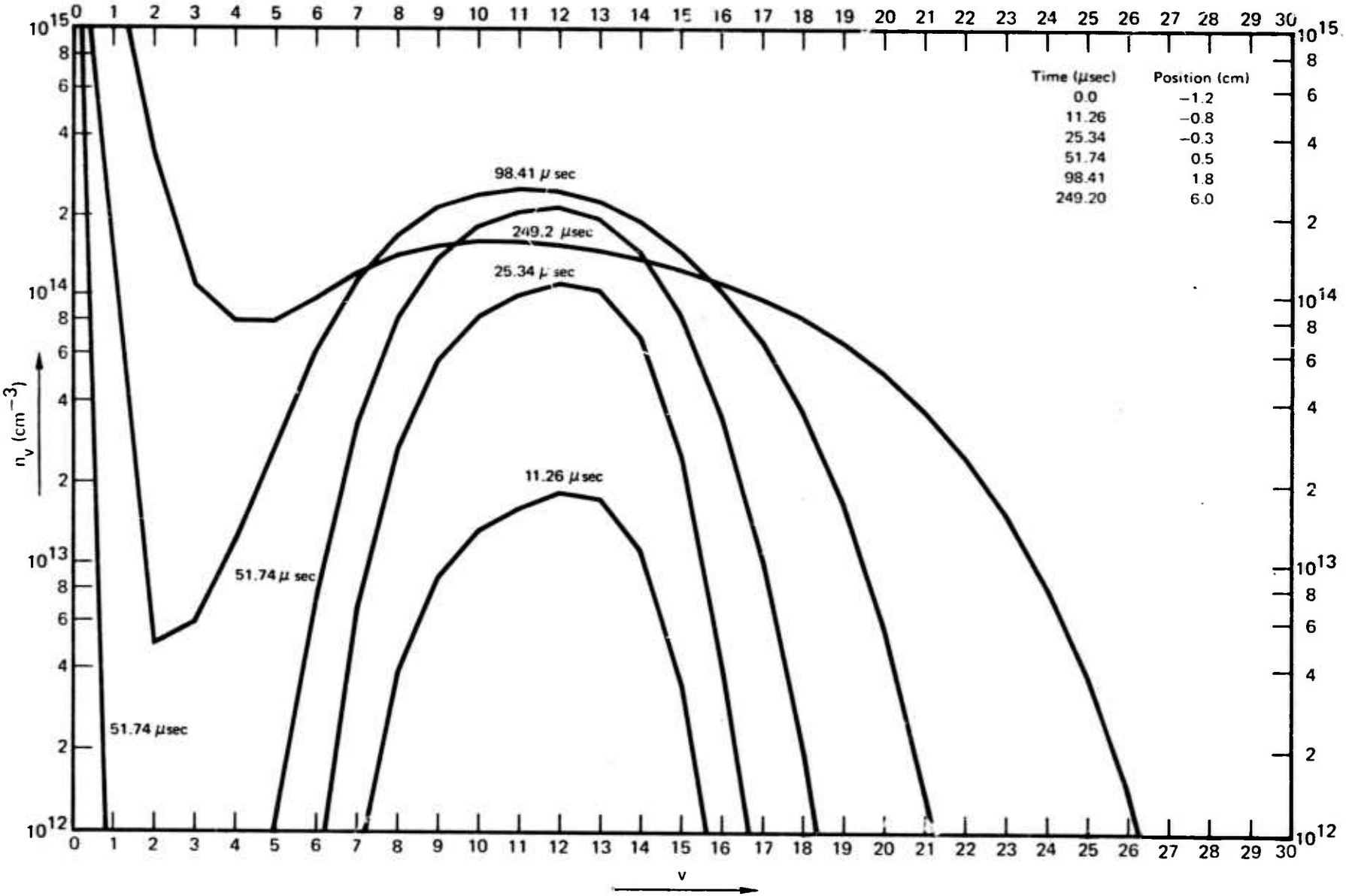

Fig. 25 CO* population distributions for Case II (with CO (300 K) injection at x = 0.0).

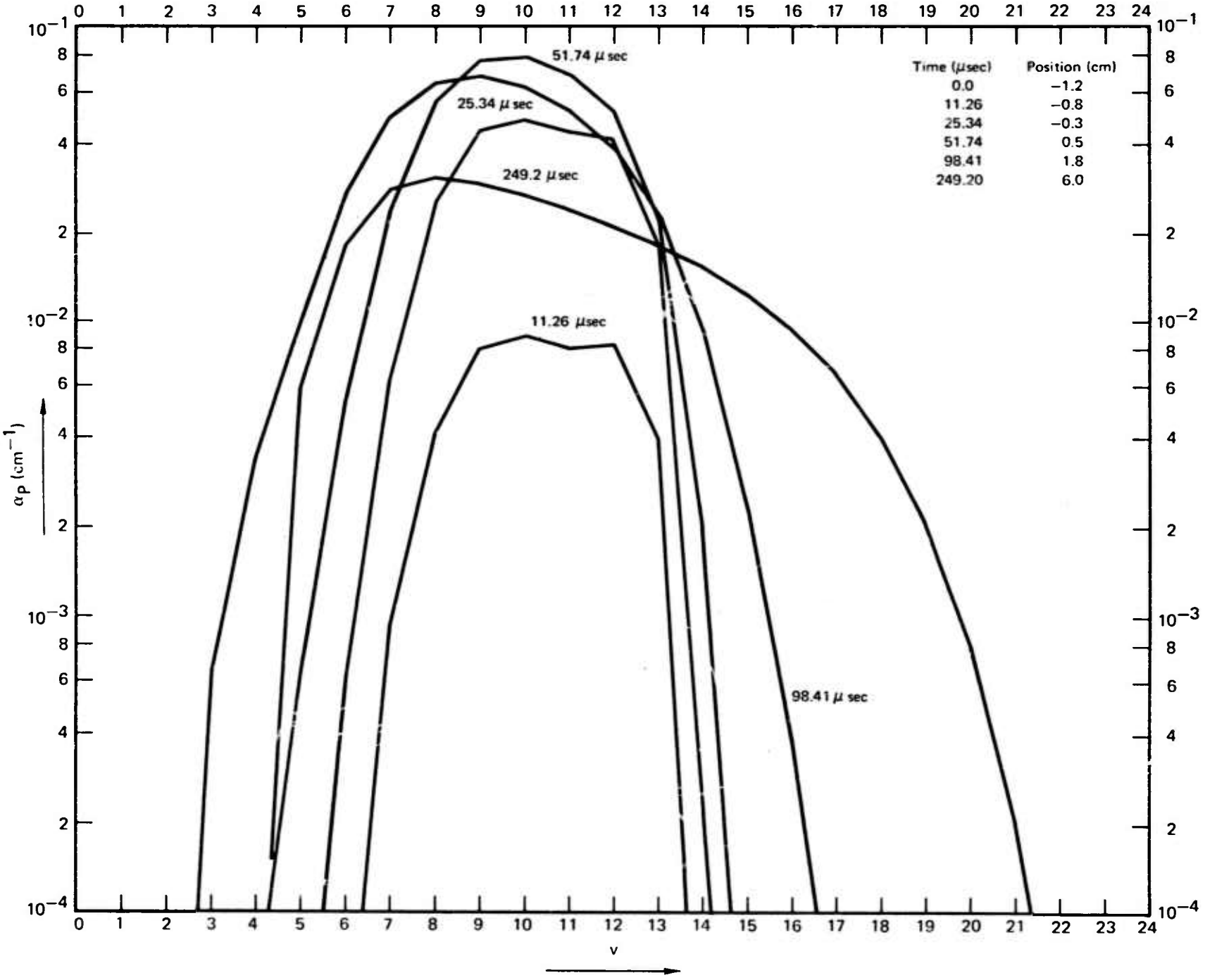

Fig. 26 Maximum P-branch gains from Fig. 25.

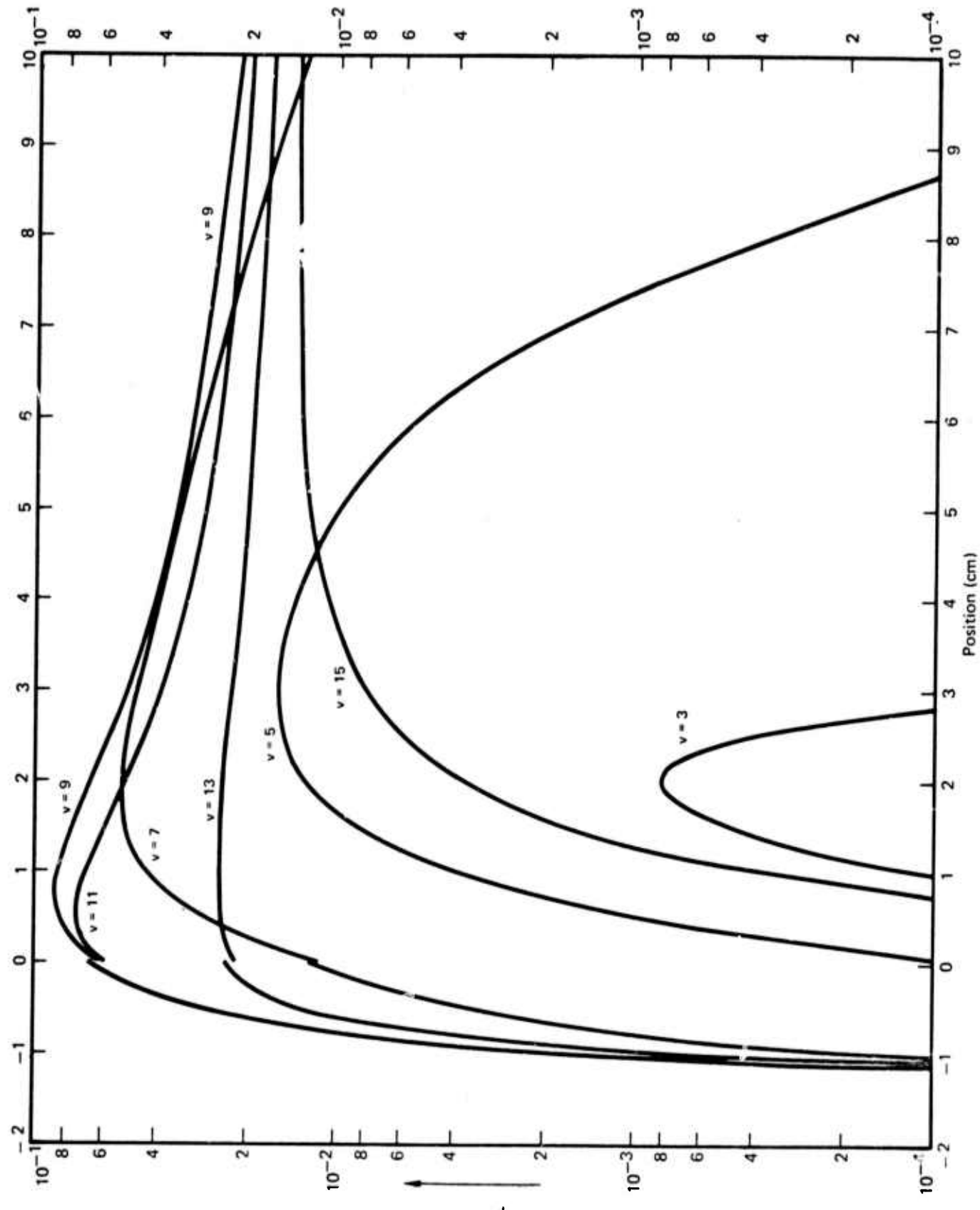

Fig. 27 Maximum P-branch gains versus position from the population distributions of Fig. 25.

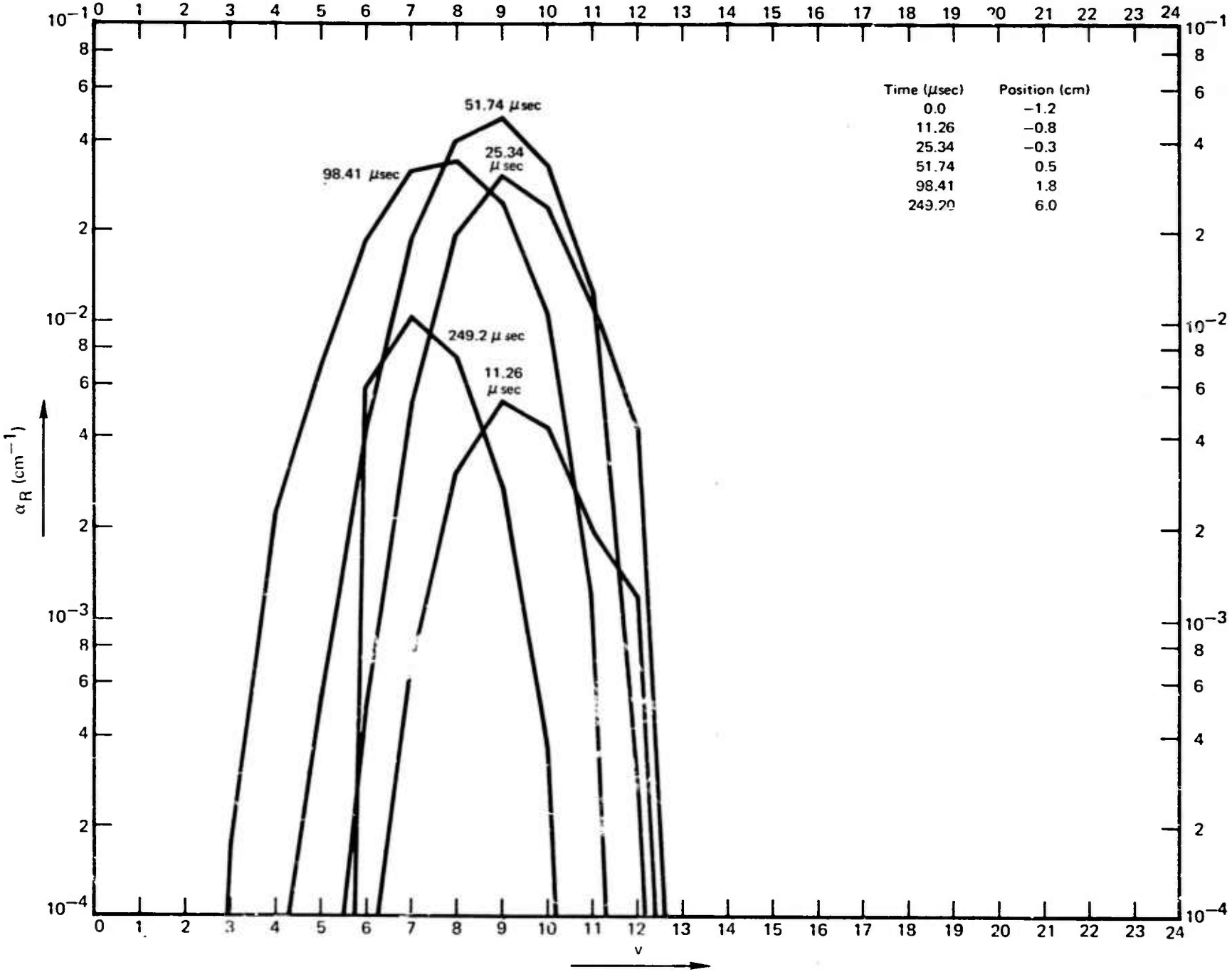

Fig. 28 Maximum R-branch gains from Fig. 25

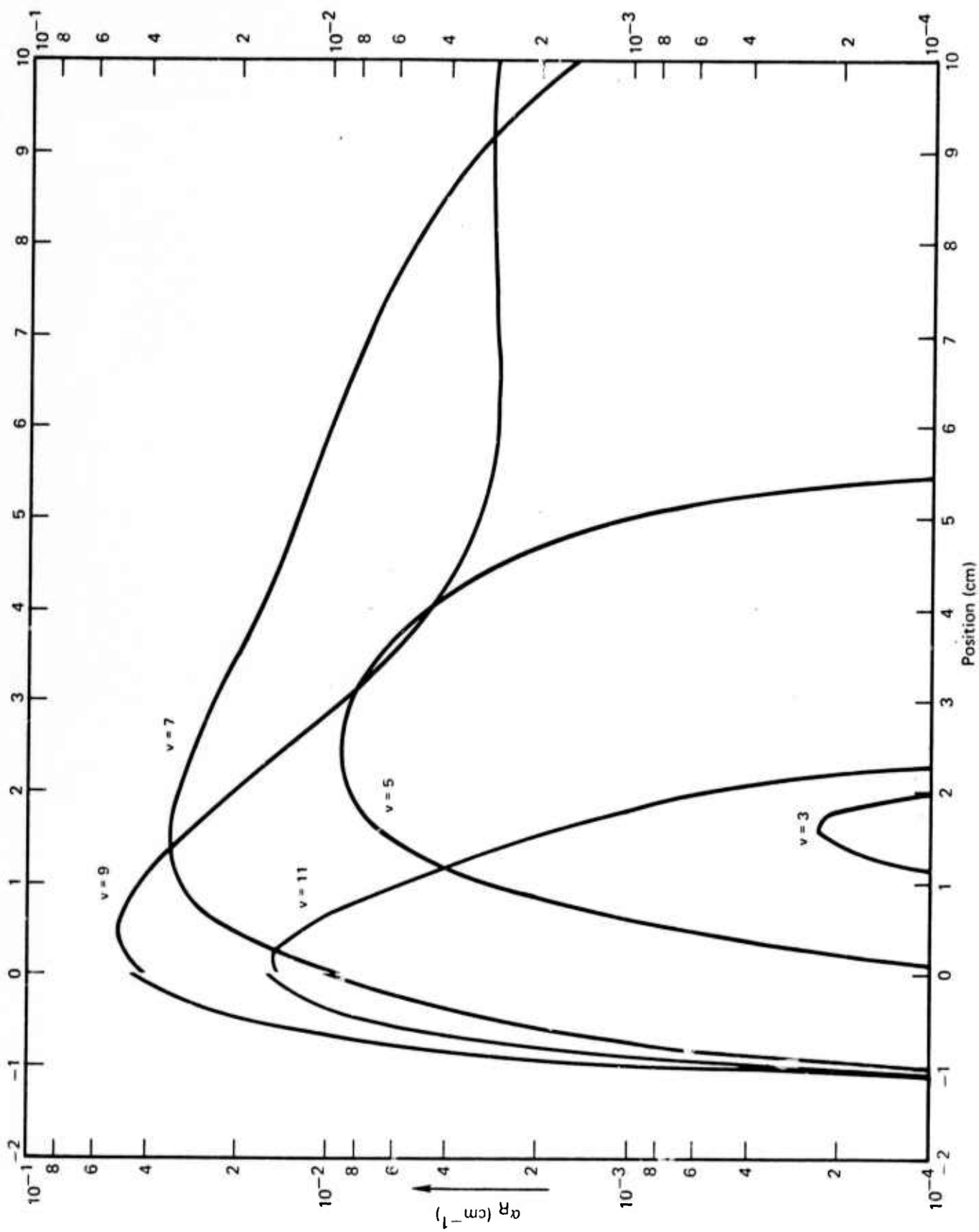

Fig. 29 Maximum R-branch gains versus position from Fig. 25.

III. REFERENCES

1. Carbon Monoxide Chemical Laser Research, First Quarterly Technical Report, Contract DAA[illegible]-72-C-0578, 23 February 1972 - 1 June 1972.
2. W. Q. Jeffers and J. D. Kelley, J. Chem. Phys. 55, 4433 (1971).
3. J. D. Kelley, J. Chem. Phys. 56, 6108 (1972).
4. K. J. Herzfeld and T. A. Litovitz, Absorption and Dispersion of Ultrasonic Waves (Academic Press, New York, 1959).
5. G. Hancock and I. W. M. Smith, Appl. Opt. 10, 1827 (1971).
6. G. Hancock, C. Morley, and I. W. M. Smith, Chem. Phys. Letters 12, 193 (1971).
7. G. Hancock and I. W. M. Smith, Trans. Faraday Soc. 67, 2586 (1971).
8. L. A. Young and W. J. Eachus, J. Chem. Phys. 44, 4195 (1966).
9. W. Q. Jeffers and C. E. Wiswall, Appl. Phys. Letters 17, 67 (1970).
10. W. Q. Jeffers and C. E. Wiswall, J. Appl. Phys. 42, 5059 (1971).
11. W. Q. Jeffers, Appl. Phys. Letters 21, 267 (1972).
12. A. A. Westenberg and N. deHaas, J. Chem. Phys. 50, 707 (1969).
13. R. D. Suart, P. H. Dawson, and G. H. Kimbell, J. Appl. Phys. 43, 1022 (1972).
14. K. H. Homann, G. Krome, and H. Gg. Wagner, Ber. Bunsenges. Physik. Chem. 72, 998 (1968); 74, 654 (1970).
15. D. D. Davis, R. B. Klemm, and M. Pilling, Intl. J. Chem. Kinetics 4, 367 (1972).

16. S. Tsuchiya, N. Nielsen, and S. H. Bauer, Paper MC1, 3rd Conference on Chemical and Molecular Lasers, St. Louis, Missouri, May 1972.